

Yarkovsky/YORP chronology of asteroid families

D. Vokrouhlický^{a,*}, M. Brož^a, W.F. Bottke^b, D. Nesvorný^b, A. Morbidelli^c

^a *Institute of Astronomy, Charles University, V Holešovičkách 2, 18000 Prague 8, Czech Republic*

^b *Southwest Research Institute, 1050 Walnut St., Suite 400, Boulder, CO 80302, USA*

^c *Observatoire de la Côte d'Azur, BP 4229, 06304 Nice Cedex 4, France*

Received 23 September 2005; revised 8 December 2005

Available online 7 February 2006

Abstract

Asteroid families are the byproducts of catastrophic collisions whose fragments form clusters in proper semimajor axis, eccentricity, and inclination space. Although many families have been observed in the main asteroid belt, only two very young families, Karin and Veritas, have well-determined ages. The ages of other families are needed, however, if we hope to infer information about their ejection velocity fields, space weathering processes, etc. In this paper, we developed a method that allows us to estimate the ages of moderately young asteroid families (approximately in between 0.1 and 1 Gyr). We apply it to four suitable cases—Erigone, Massalia, Merxia, and Astrid—and derive their likely ages and approximate ejection velocity fields. We find that Erigone and Merxia were produced by large catastrophic disruption events (i.e., parent body ≥ 100 km) that occurred approximately 280 and 330 Myr ago, respectively. The Massalia family was likely produced by a cratering event on Asteroid (20) Massalia less than 200 Myr ago. Finally, the Astrid family, which was produced by the disruption of a 60–70 km asteroid, is 100–200 Myr old, though there is considerable uncertainty in this result. We estimate that the initial ejection velocities for these families were only a few tens of meters per second, consistent with numerical hydrocode models of asteroid impacts. Our results help to verify that asteroid families are constantly undergoing dynamical orbital evolution from thermal (Yarkovsky) forces and spin vector evolution from thermal (YORP) torques.

© 2006 Elsevier Inc. All rights reserved.

Keywords: Asteroids, dynamics; Thermal effects

1. Introduction

Asteroid families, defined as a collection of bodies with similar proper semimajor axes a , eccentricities e , and inclinations I , have received increasing attention over the past several decades (e.g., Bendjoya and Zappalà, 2002; Cellino et al., 2002; Zappalà et al., 2002). Families are produced by asteroid collisions, with the ejected fragments making up the members of the family. They are important to small body studies for many reasons. Spectroscopic observations allow one to use families to study the mineralogical structure of various parent bodies (e.g., Cellino et al., 2002). Families can also be used to study the outcomes of disruption events over a size range otherwise inaccessible to laboratory experiments (e.g., Durda et al., 2004).

Finally, the number of observed families and their production rate can be used to constrain the collisional history of the main belt (Bottke et al., 2005a, 2005b).

Extracting useful information from asteroid families, however, is not always straightforward. For example, many observed family members have had their spectroscopic properties affected by space weathering processes (e.g., Chapman, 2004; Jedicke et al., 2004; Nesvorný et al., 2005). Some families reside in highly populated regions of the main belt, such that discriminating family members from interlopers can be difficult to impossible (e.g., Migliorini et al., 1995). Similarly, family members undergo collisional evolution over time, forcing the size frequency distribution of the population to slowly evolve toward the same shape as the background population (Bottke et al., 2005a, 2005b). Finally, their initial configuration in (a, e, I) space, set by their ejection velocity from the family, undergoes modifications over time via gravitational and non-gravitational perturbations (e.g., Bottke et al., 2001, 2002; Nesvorný et al.,

* Corresponding author. Fax: +420 2 21 91 25 67.
E-mail address: vokrouhl@mbox.cesnet.cz (D. Vokrouhlický).

2002a; Carruba et al., 2003, 2005). In this manner, older families evolve and gradually obscure their initial velocity field. These same effects can even erase the signatures of small families, making it difficult to use them as constraints in modeling the evolution of the main belt (e.g., Marzari et al., 1999; Bottke et al., 2005a). A common problem affecting all of these issues is the unknown age of these families, which can make it difficult to determine how much collisional and dynamical evolution has taken place in individual families since their creation. Thus, to understand asteroid families, we need some means of estimating their ages.

To deal with this issue, several groups have proposed methods to estimate asteroid family ages (e.g., Nesvorný et al., 2005 or Vokrouhlický et al., 2005, and references therein). Perhaps the most straightforward means is to count craters on the surface of asteroids imaged by spacecraft and then compute the surface age using estimates of the crater production rate (e.g., Belton et al., 1992, 1994; Greenberg et al., 1994, 1996; Chapman, 2002). This has been accomplished for several family asteroids, including (951) Gaspra in the Flora family and (243) Ida in the Koronis family. (951) Gaspra is believed to have an age of 50–300 Myr (Veverka et al., 1994; Greenberg et al., 1994; Chapman et al., 1996b). It is more difficult to estimate an age for (243) Ida, whose craters are close to empirical saturation; best estimates suggest it is over 2 Gyr old (Chapman et al., 1996a; Greenberg et al., 1996). If these bodies have not experienced post-family-formation disruption events, their crater surfaces ages should also represent the family's age. Unfortunately, estimating asteroid ages from craters can be problematic, with many unknown or poorly constrained factors (e.g., the unknown scaling relationship needed to turn projectiles into craters, the poorly understood effects of crater erasure mechanisms, the production population, etc.). Obviously, they also depend on rare visits to asteroids by spacecraft.

Another procedure, which works well for young families, is to track the orbital evolution of the family members backwards in time all the way to their starting orbits. The main obstacle here is obtaining a large enough sample of asteroid proper elements (e.g., Knežević and Milani, 2000, 2003; Knežević et al., 2002) to compute when the fragments all shared the same approximate starting orbit (note young families are statistically expected to be in the same time small). Modern observational programs and computational efforts have allowed the database of proper elements to greatly expand over the past decade (<http://newton.dm.unipi.it/>), such that many small, young families can now be identified for the first time. Using this method, Nesvorný et al. (2002b, 2003) determined that the Karin cluster, a group of asteroids produced by the disruption of a diameter $D \approx 30$ km body, was 5.75 ± 0.05 Myr old (see also Nesvorný and Bottke, 2004). This method was also successfully applied to the Veritas family, which was found to have an age of 8.3 ± 0.5 Myr (Nesvorný et al., 2003). Note that Milani and Farinella (1994) had also suggested that the Veritas family may be less than 50 Myr old based on the dynamical instability of some of its members in resonances. Unfortunately, this direct integration age-determination method is limited to families younger than about 10 Myr. It may also not work at all

if the zone where the family resides is highly chaotic (e.g., the Iannini family, see Nesvorný et al., 2003).¹

A third method is to use the spin axis distribution of a family to deduce its age. This can only be accomplished in certain special circumstances. For example, Slivan (2002) and Slivan et al. (2003) found that many $20 < D < 40$ km Koronis family members have an unusual spin vectors, with the prograde rotators having obliquities between 42° to 50° and nearly identical spin periods (7.5–9.5 h) and the retrograde rotators having obliquities between 154° to 169° and spin periods less than 5 h or greater than 13 h. As will be discussed further below, Vokrouhlický et al. (2003) showed these spin vectors had been affected by long-term thermal torques that caused them to evolve into their current states over several Gyr (i.e., YORP torques; Rubincam, 2000). Vokrouhlický et al. estimated from these results that the Koronis family was likely ~ 2.5 Gyr, in agreement with the cratering record observed on Ida (e.g., Chapman, 2002) and the large dynamical spread of the family (e.g., Bottke et al., 2001).

A fourth way to estimate asteroid family ages is to model the evolution of their size frequency distributions and compare it observations (e.g., Marzari et al., 1995, 1996, 1999). For example, Marzari et al. (1995) fit for the size distribution of the Koronis and Themis asteroid populations, determining an age for both exceeding ~ 2 Gyr. Potential caveats of this method are: (i) the unknown initial size distribution in each family, and (ii) the parameters that govern collisional evolution in the main belt, many which have been poorly known until recently (e.g., the shape and nature of the main-belt size distribution over the last 4 Gyr, the scaling law that controls asteroid breakup events, etc.). These factors, if not accounted for correctly, can lead to inaccurate family age estimates.

Finally, Farinella and Vokrouhlický (1999) introduced the idea that the ages of asteroid families might be measured by estimating how long they take to disperse via Yarkovsky thermal forces. As we will describe in more detail below, their method was based on the idea that small family members drift more quickly in semimajor axis than large family members. In many cases, this non-uniform dispersal can be used like a clock to estimate the family's age. Vokrouhlický et al. (2002) used this idea to estimate that the Eos family was ~ 2 Gyr old, while Nesvorný et al. (2003, 2005) and Carruba et al. (2003) estimated the ages of several additional asteroid families. A problem with these age estimates, however, is that they did not account for the initial ejection velocities of the family fragments nor how YORP thermal torques affect their spin vectors (and hence their Yarkovsky drift rates). Using a more refined

¹ A “less-ambitious variant” of the direct backward integration of orbits was originally proposed by Brouwer (1951) who noted that the sum of proper longitude of ascending node Ω_p and proper longitude of pericenter ω_p is stationary in the linearized perturbation theory. Any clustering in this sum, presumably only slowly dispersing due to higher-order perturbation terms, was seen as a signature of the family's young age. Brouwer (1951) thus argued for the young age of the Eos family. A critical reassessment of the argument by Farinella et al. (1989) and Vokrouhlický et al. (2005), however, showed some problems with this method. Note that young families such as Karin or Iannini have $(\Omega_p + \omega_p)$ values that are strongly clustered.

method (that will be described in detail below), Vokrouhlický et al. (2005) estimated that the Eos family age was $1.3_{-0.2}^{+0.15}$ Gyr, younger than previous estimates.

The purpose of this paper is to compute the chronology of several asteroid families using a more sophisticated model than that described above. By involving “the other face of thermal phenomena,” namely YORP thermal torques that affect an asteroid’s rotation, we believe we now have the means to distinguish the initial ejection velocity distribution of the family from its Yarkovsky-driven dispersion. Our results for those families modeled in this paper indicate that 30–50% of their current spread in semimajor axis was produced by their initial ejection velocity distribution. This result is in reasonable agreement with an independent analysis of Dell’Oro et al. (2004), who determined using statistical methods that the initial families were $\simeq 30\text{--}50\%$ smaller than the observed families. Our approach, however, can also be used to determine family ages with more precision than before. Additional useful information, such as the initial spread of the families or the average strength of Yarkovsky thermal torques on given-sized asteroids, can be also derived from our work.

Section 2 introduces our method. In Sections 3 and 4, we apply this new method to selected families; first we characterize them anew as clusters in proper element space using an up-to-date orbital catalog, and then we determine their ages. In Section 5, we computed the orbital evolution of our families by tracking how test asteroids placed in the family evolve via Yarkovsky thermal forces. These results illustrate how some migrating objects interact with weak mean motion resonances. Finally, in Section 6 we discuss the limitations of our method and why it cannot be used for all observed asteroid families.

2. The method

Asteroid families are usually recognized as statistically significant clusters in the proper orbital element space: semimajor axis a , eccentricity e , and inclination I . Various cluster identification methods have been developed to locate families (e.g., Bendjoya and Zappalà, 2002). Additional information needed to understand the evolution of asteroid families is the size frequency distribution (SFD) of their members. A family’s SFD experiences collisional evolution from the moment it was formed in the main belt to the present day.

Yarkovsky thermal forces affect families in two important ways: (i) they secularly affect the semimajor axis of the family members, causing them to disperse in semimajor axis (e.g., Vokrouhlický, 1998; Vokrouhlický and Farinella, 1998, 1999), and (ii) the induced da/dt drift rates are size-dependent. As a result, Yarkovsky forces differentially expand each family in semimajor axis–diameter (a, D) space. Evolution in eccentricity and inclination space (e, I) is generally negligible unless the body in question is interacting with a resonance (e.g., Nesvorný and Morbidelli, 1998; Morbidelli and Nesvorný, 1999; Bottke et al., 2001; Nesvorný et al., 2002a; Vokrouhlický and Brož, 2002). In this paper, we concentrate on the evolution of younger families that typically have not yet reached any important resonances. For this reason, we do not further discuss (e, I) evo-

lution in this paper. Similarly, we assume that young families have experienced minimal comminution since their formation.

Many asteroid families exhibit a characteristic pattern when their members are projected onto a plane defined by semimajor axis a and absolute magnitude H (which can be converted to D once an albedo has been selected). The largest asteroid resides near the mean value of a for the whole family, while the extreme values of a are occupied by the smallest asteroids. Because this configuration matches our expectation of what asteroid collisions should produce, namely that small fragments created by a family-forming event have higher ejection velocities than larger ones, Cellino et al. (1999) attempted to use these data to calibrate the unknown velocity–size relation. Their work assumed that families, since their formation, have not dynamically evolved in a . (Note that this work was a follow-up to an earlier study by Zappalà et al. (1996), except for recognizing that proper e and I might be unstable over the long-term via effects from weak resonances.) Dynamical studies invoking the Yarkovsky effect, however, have shown that families do disperse with time. Our work here allows us to evaluate various parameters related to this dispersion. In particular, we infer their age and initial spreading on which eventually the Cellino et al. (1999) considerations can be applied.

2.1. General considerations

We start here with general considerations and then proceed from simple to more sophisticated models. Consider a projection of the family members onto the (a, H) plane. In general, the result is a clump of data points. In a model whose goal is to quantitatively understand this distribution and infer the initial velocity field or Yarkovsky dispersal scenario, we need to use some parametric relationship between H and a , say $H = H(a; p_1, p_2, \dots)$, where (p_1, p_2, \dots) are parameters. When this functional representation is a one-to-one mapping achieved by fixing all but one parameter, say p_n , we can characterize the family with the distribution function $\mathcal{D}(p_n)$ over some interval of p_n values:

$$\mathcal{D}(p_n) = \frac{dN}{dp_n}, \quad (1)$$

where dN is number of family asteroids in the (a, H)-strip generated by changing p_n in the range ($p_n, p_n + dp_n$). Function $\mathcal{D}(p_n)$ then contains all of the family’s information within the model.

The most general (yet simple) parametric relation we shall consider in this paper is given by

$$0.2\beta H = \log(\Delta a/C), \quad (2)$$

with $\Delta a = a - a_c$; we argue in Section 2.3 that this form is tailored toward the Yarkovsky dispersion model. Equation (2) gives H as a function of a using three parameters $H = H(a; \beta, a_c, C)$: (i) β is positive, (ii) a_c essentially shifts the origin of the family in a , and (iii) C can acquire both negative and positive values over some interval. In the application described below, we fix β and a_c and then consider the density function $\mathcal{D}(C)$ of the last parameter C .

2.2. Toy model 1: Initial dispersion of fragments

Let us start with a simple, unrealistic model of a family represented by the initial distribution of ejecta produced by the disruption of a parent body. Assuming the latter resides on near-circular orbit with semimajor axis a_c , such that we can neglect eccentricity corrections in the following equations, we assume that a fragment ejected with a transverse velocity V_T is thrown onto an orbit with:

$$\Delta a = \frac{2}{n} V_T + \mathcal{O}(e) \quad (3)$$

with respect the orbit of the parent body (i.e., $\Delta a = a - a_c$ as above). Here n is the heliocentric mean motion of the parent body.

Next, we assume

$$V_T = V_0 \left(\frac{D_0}{D} \right)^\beta \cos \alpha, \quad (4)$$

where D is the size of the body, D_0 and V_0 are some reference values and α is directional cosine of the fragment's velocity with respect the transverse direction to the parent body orbit.² The velocity V_0 and the (positive) exponent β are a priori unknown parameters. Data from the young Karin cluster are consistent with $\beta \simeq 1$ (Nesvorný et al., 2002b), while several papers considered analytical arguments in favor of particular β values (e.g., $\beta \simeq 3/2$; Cellino et al., 1999). Equation (4) is highly idealized because it assumes that bodies of size D were ejected with the same velocity $V_0(D_0/D)^\beta$. We convert absolute magnitude H to size D using the relation $D = D_0 \times 10^{-0.2H} / \sqrt{p_V}$, with $D_0 = 1329$ km the reference size value and p_V the geometric albedo in the optical band. Assuming p_V is size-independent, the family members are distributed in (a, H) space according to Eq. (2) with

$$C = \frac{2}{n} V_0 p_V^{\beta/2} \cos \alpha = C_0 \cos \alpha. \quad (5)$$

For the moment, we assume the fragments are ejected isotropically in space. Here $\cos \alpha$ is uniformly distributed in the interval $(-1, 1)$ and thus C acquires uniform values between $-C_0$ and C_0 . For the same reason, the density function $\mathcal{D}(C)$ is constant (note we write $\mathcal{D}(C) = dN/dC = (dN/d\cos \alpha)(d\cos \alpha/dC)$ and each of these two multiplicative factors is constant). The simple form of this result means the functional relation $H(a)$, as given in Eq. (2), is well suited (optimized) for this model.

Perhaps the most restrictive assumption above is that of constant ejection velocity for fragments of a given size D . There is likely to be some velocity dispersion, even for fragments of the same size; this factor makes the previous analysis more complicated. Petit and Farinella (1993) show an example of how to model this effect. They give the transverse velocity V_T as a Gaussian function with the half-width parametrically depending on the size of the fragment. In this situation, the template

relation (2) is no longer tailored to the model yet it can still be formally used to define the density function $\mathcal{D}(C)$ of the formal parameter C . Numerical results indicate that within this model $\mathcal{D}(C)$ is not constant over a finite interval of values but instead has a maximum for $C = 0$ and drops to zero when $|C| \rightarrow \infty$. Similarly, if the initial velocity is not isotropic but contains a preferred direction, $\cos \alpha$ is not uniform and this produces variations in $\mathcal{D}(C)$. This result is frequently seen in numerical simulations (e.g., Love and Ahrens, 1996; Ryan and Melosh, 1998; Benz and Asphaug, 1999; Michel et al., 2001, 2002) and is also supported by analysis of young clusters like Karin or Veritas.

2.3. Toy model 2: Yarkovsky diffusion

Our second toy model illustrates the basic features of the Yarkovsky dispersion scenario. Here we assume all family asteroids have the same initial value of the semimajor axis a_c with their initial spin axes randomly oriented in space and kept fixed in time. Most of these assumptions are false. For example, spin vectors change with time because of collisional and dynamical effects (such as thermal and gravitational torques).

Yarkovsky forces cause each family asteroid to evolve to a new value of the semimajor axis $a = a_c + (da/dt)T$, where da/dt is the rate of change in semimajor axis and elapsed time is T . For asteroids larger than $\simeq 50$ m, and for reasonable surface thermal properties, $(da/dt) \propto D^{-1}$ (e.g., Bottke et al., 2002). Moreover, the diurnal variant of the Yarkovsky effect is likely to dominate (da/dt) over the seasonal variant by at least an order of magnitude. Denoting spin axis obliquity ϵ , we have $(da/dt) \propto \cos \epsilon$ (thus $|\kappa_1| \gg |\kappa_2|$ in Eq. (8)). Choosing an arbitrary reference size D_0 , (da/dt) becomes dependent on two parameters; $(da/dt) = (da/dt)_0(D_0/D) \cos \epsilon$, with $(da/dt)_0$ the maximum Yarkovsky drift rate for a body of size D_0 (with zero obliquity). For convenience, we assume $D_0 = 1329$ km as above. Assuming all asteroids have the same geometric albedo p_V , each in time T reach a point (a, H) so that

$$0.2H = \log(\Delta a/C), \quad (6)$$

with $\Delta a = a - a_c$ and

$$C = \sqrt{p_V} (da/dt)_0 T \cos \epsilon = C_0 \cos \epsilon. \quad (7)$$

Note Eq. (6) again has the same functional form as Eq. (2), with $\beta = 1$ a direct consequence of the size dependence of da/dt . In our model $\cos \epsilon$ has a uniform distribution in the interval $(-1, 1)$, thus again C acquires uniform values in the interval $(-C_0, C_0)$. It also follows that $\mathcal{D}(C)$ is constant over the same interval of values. With p_V fixed, the limiting values C_0 directly constrains the family's age T . This representation was used by Vokrouhlický et al. (2002) and Nesvorný et al. (2003, 2005) to estimate the ages of several families (e.g., Eos).

2.4. Toward a more general model

To a large degree, both toy models from Sections 2.2 and 2.3 yield similar results: when a moderate dispersion velocity and $\beta \simeq 1$ are used, both predict a nearly constant $\mathcal{D}(C)$ distribution

² Ideally, the ejection velocity field should be related to the center of mass frame of the parent body and projectile. For simplicity, we neglect this correction. The relevant formulas can be found, e.g., in Marzari et al. (1995).

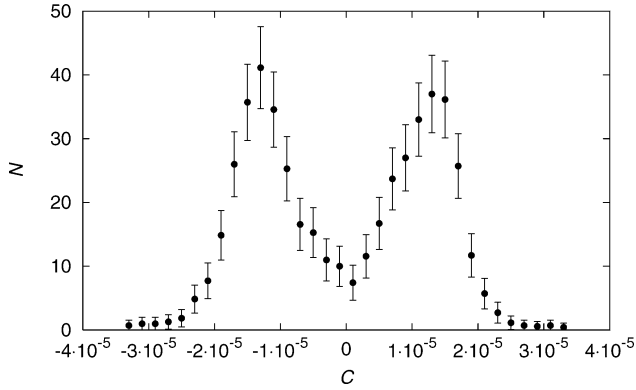


Fig. 1. Symbols show number $N_{\text{obs}}(C)$ of observed Erigone members in $(C, C + \Delta C)$ bins with error-bars given as $\sqrt{N_{\text{obs}}(C)}$. We chose $\Delta C = 2 \times 10^{-6}$ AU and a_c uniformly averaged in the range $(2.368, 2.374)$ AU. Though not perfect $N_{\text{obs}}(C)$ is approximately symmetric about $C = 0$ with significant maxima at $C = \pm 1.5 \times 10^{-5}$ AU.

function. Real families, however, are more complex, producing characteristic features in the distribution function $\mathcal{D}(C)$ that allow us to discriminate between the two toy approaches. From this point of view our work will concentrate on these features for several selected families (see also the analysis of the Eos family by Vokrouhlický et al., 2005).

To demonstrate our method, we start with the Erigone family whose $\mathcal{D}(C)$ is shown in Fig. 1. Here we plot the number $N_{\text{obs}}(C)$ of Erigone members in the interval $(C, C + \Delta C)$ values. We assume $\Delta C = 2 \times 10^{-6}$ AU; note $N_{\text{obs}}(C)$ is identical to $\mathcal{D}(C)\Delta C$ and for simplicity we shall use $N_{\text{obs}}(C)$ in this paper. A notable feature of this distribution, incompatible with either of the toy models described above, are maxima at $C \simeq \pm 1.5 \times 10^{-5}$ AU which are apparently symmetric about the origin. The value $N_{\text{obs}}(0)$ represents only about 25% of the maximum value at a high statistical level (we use $\sqrt{N_{\text{obs}}(C)}$ as quasi-errors of the values $N_{\text{obs}}(C)$ in each of the bin in C).

These $N_{\text{obs}}(C)$ maxima are a direct consequence of the fact that small asteroids tend to preferentially populate regions at the outskirts of the family while leaving its center underpopulated (Fig. 4 shows the (a, H) projection for Erigone). This distorted fragment distribution is hard to reconcile with any reasonable ejection field produced by the family-forming event. In particular, it would mean two anti-aligned fragment streams are thrown away from the impact site such that they preferentially populate extreme V_T values. This geometry has yet to be observed in numerical simulations of asteroid collisions (e.g., Durda et al., 2004) nor would it be expected from heuristic arguments. It might seem plausible that the family’s central depletion is caused by dispersal via weak resonances, but, as we will show below, this explanation is not observed in our numerical integration results (Section 5.1). Instead, we argue that the Yarkovsky dispersal model offers a more natural explanation for this feature.

In order to understand how this unusual family configuration was produced, we not only need to invoke the Yarkovsky effect but also the Yarkovsky–O’Keefe–Radzievskii–Paddack (YORP) effect (e.g., Rubincam, 2000; Vokrouhlický and Čapek,

2002; Bottke et al., 2002). YORP, a variant of the same thermal phenomenon that causes asteroids to drift in semimajor axis, describes how thermal torques affect the rotation state of irregularly shaped bodies. If given sufficient time, YORP can preferentially tilt the obliquity values of asteroids toward extreme values (i.e., 0° and 180° ; Čapek and Vokrouhlický, 2004). As asteroids approach these asymptotic obliquity states, their rotation rates are either accelerated or decelerated. This somewhat simplistic picture of the long-term evolution of an asteroid’s rotation state may be altered, albeit temporarily, by spin-orbit secular resonances. Evidence for the combined effect of YORP and spin-orbit resonances has been found among Koronis family members (e.g., Slivan, 2002; Vokrouhlický et al., 2003).

At present, the nature of YORP evolution near the asymptotic values (or, for lack of a better phrase, near their end-states) is poorly understood. A steady deceleration of an asteroid’s rotation rate should result in the onset of a tumbling rotation state or it should drain enough rotational angular momentum from the body that a random collision could efficiently reestablish a nominal rotation state. For fast rotating asteroids, they should eventually undergo fission or they should undergo shape changes that weaken or even turn off the YORP effect (i.e., morphing the body into a symmetrical shape would turn off YORP). Neither end-state has been studied enough to include them into our analysis of asteroid families. For this reason, we will neglect them in this paper.

The principal effect of YORP in our model will be its ability to preferentially tilt the obliquity values of family members toward extreme values that, in turn, affect the semimajor axis drift rates of the bodies via the Yarkovsky effect. As we will show, the combined effects allow small family asteroids to evolve toward the extreme borders of the family. In Section 4, we have devised a numerical scheme to quantitatively test this idea.

3. Selected families: HCM identification

We start by applying a hierarchical clustering method (HCM; e.g., Bendjoya and Zappalà, 2002, and references therein) to identify members of asteroid families as tight clouds of asteroids in proper element space.³ We used analytically-determined proper elements of nearly 170,000 main belt numbered and multi-opposition asteroids from AstDyS database (<http://www.dm.unipi.it/>) as of November 2004. We adopt the “standard metric” of Zappalà et al. (1990, 1995) to define the relative velocity between two orbits and then proceed to identify families with some cut-off value V_c . Tested V_c values are typically between 20 to 110 m/s, with the lower range corresponding to the uncertainty in the analytic proper elements. As we will described below, choosing the appropriate V_c value to discriminate a family from the background population is frequently a matter of experimentation.

Fig. 2 shows the four families studied in the paper in proper element space: Erigone, Massalia, Merxia, and Astrid. The

³ Our program in C language is available on <http://www.boulder.swri.edu/~davidn/>.

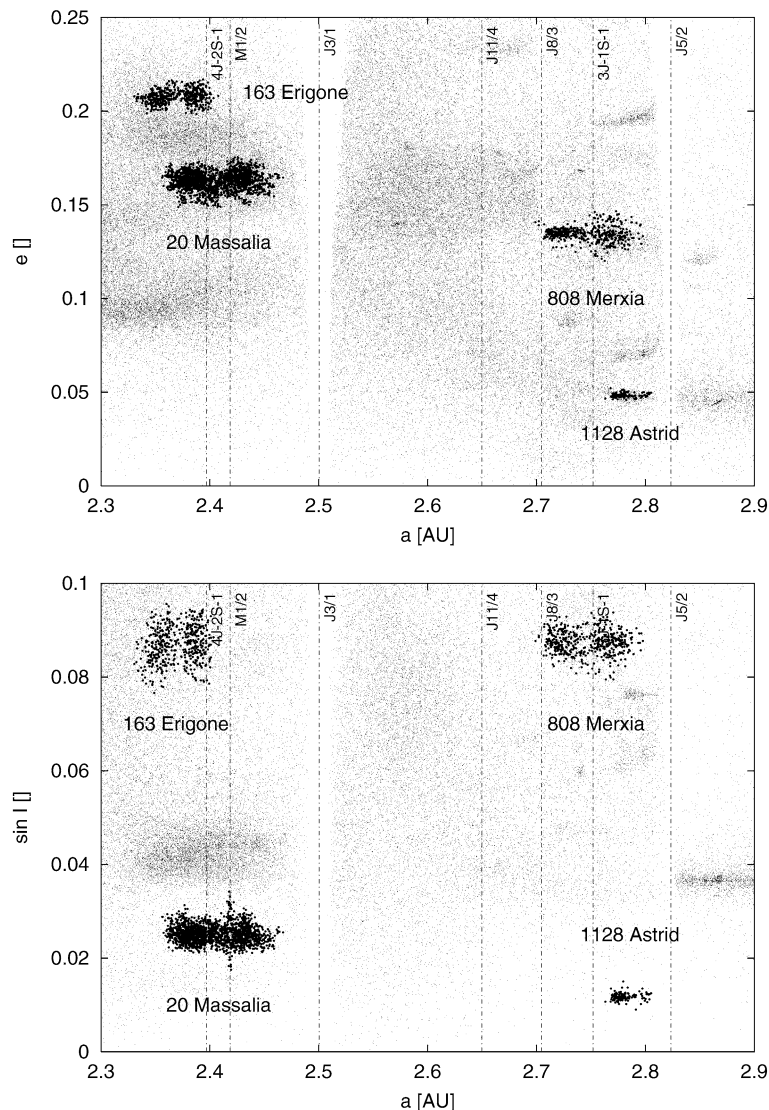


Fig. 2. Four prominent families that show concentrations of asteroids at extreme value of semimajor axis: Erigone, Massalia, Merxia, and Astrid. Here we show their nominal realizations (see the text) in the space of proper orbital elements: (i) semimajor axis a vs eccentricity e (top) and (ii) semimajor axis a vs sine of inclination $\sin I$ (bottom). We also indicate position of the major mean motion resonances with Jupiter (J3/1, J5/2, J8/3) and some of the weaker resonances (e.g., M1/2, 3J-1S-1, or 4J-2S-1). Dots are all background asteroids and other families not considered in this paper.

background population of asteroids, as well as other families not selected for this study, are shown as well. Other items displayed are the principal mean motion resonances (J3/1, J5/2, and J8/3) with Jupiter, several weaker mean motion resonances (such as J11/4, exterior resonance with Mars M1/2), and several three-body resonances (4J-2S-1 and 3J-1S-1, S stands for Saturn); the notation follows Nesvorný and Morbidelli (1998) and Morbidelli and Nesvorný (1999). Each family will be described in detail below.

3.1. Erigone

Fig. 3a shows the number of asteroids associated with the Erigone family as a function of the HCM velocity cut-off V_c . We note two important transitions occur along these data: (i) For $V_c < 54$ m/s, the cluster contains only few objects near Asteroid (163) Erigone; (ii) for $V_c \geq 80$ m/s, a large fraction of

the local asteroid belt coalesces with the family. The Erigone family is thus reasonably defined for cut-off velocities between $54 < V_c < 80$ m/s. Inside this range, the family slowly accumulates additional members. We thus decided to consider $V_c = 56$ m/s as a defining value for our “nominal” Erigone family.⁴

The cumulative distribution of absolute magnitude H values for family members can be piecewise approximated using a power-law of the form $N(< H) \propto 10^{\gamma H}$. Fig. 3b shows the values of γ as a function of V_c for the cumulative H distribution in the (13.5, 15.5) range.⁵ Interestingly, for family-defining values

⁴ Our results in this paper, such as the estimated age of the family, weakly depend on the particular choice of the HCM velocity cut-off provided it stays in a “reasonable range” about the nominal value.

⁵ The upper values in this interval might be partially affected by the observational bias, nevertheless we find our values of γ valuable. The completion

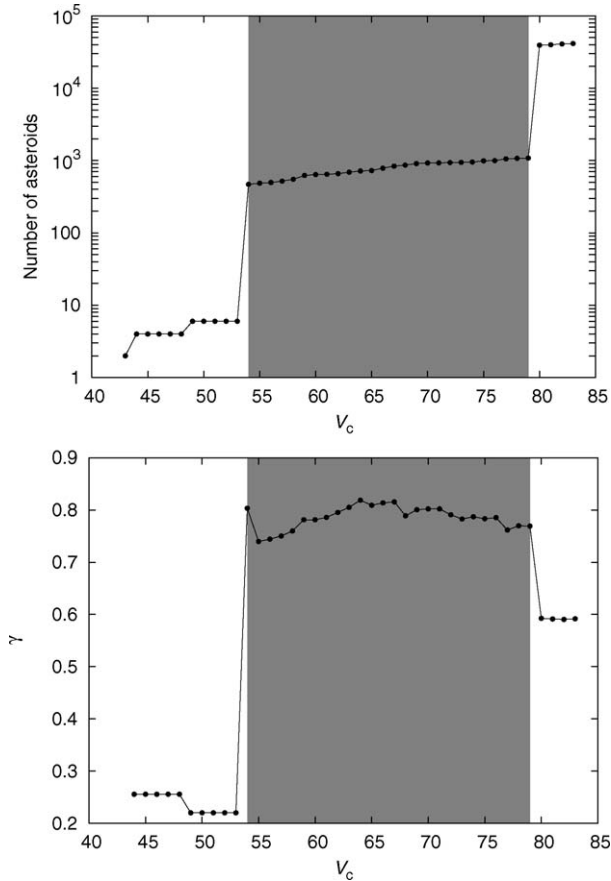


Fig. 3. Number of asteroids associated with Erigone family (top) and power-law index γ of the cumulative magnitude distribution in the range (13.5, 15.5) (bottom) as a function of the HCM cut-off velocity V_c . Two critical values of V_c are: (i) 54 m/s, when the close vicinity of (163) Erigone merges with the remaining part of the family, and (ii) 80 m/s, when the family (as formally identified with the HCM method) coalesces with bulk of the inner main belt. The family is reasonably well defined in between those two V_c values, slowly accumulating outskirts members and interlopers. In this interval, γ consistently oscillates between 0.74 and 0.8. When the bulk of the inner main belt formally associates with the family, γ acquires a value close to 0.6 (determined also by Ivezic et al. (2001) from the SDSS data).

of V_c , γ consistently oscillates between 0.74 and 0.8, yielding a value $\gamma = 0.75 \pm 0.04$ for the nominal family (see also Fig. 11, where the cumulative distributions in H for our families is shown). This rather steep value drops to $\gamma \simeq 0.6$ when the background population of asteroids coalesces with the family for $V_c \geq 80$ m/s (Fig. 3). This limiting value agrees with the result of Ivezic et al. (2001), who found $\gamma \simeq 0.61$ for asteroids in the absolute magnitude range (13, 15), a value possibly dominated by inner main-belt objects. The relative steepness of the Erigone H distribution here with respect to the background could indicate that the family is young. On the other hand, recent work indicates that the power law slope of some asteroid families for $H < 15$ is not seriously modified by collisions, even when the families are several Gyr (Bottke et al., 2005b). At $H \geq 15.5$, the steep H -distribution becomes shallower, mim-

icking the background asteroid population (see Morbidelli et al., 2003). The change in slope is an artifact of comminution (Bottke et al., 2005b) and observational bias; it is found in all the families discussed in this paper.

Fig. 4 shows our nominally identified Erigone family in proper (a , e), proper (a , $\sin I$) and (a , H). One of the most interesting features, common to all the families selected for study in this paper, is a central depletion of the family (see Section 2.4). It is most easily seen in the (a , H) projection. This feature cannot be attributed to any diffusive resonances (Section 5.1); the only relevant nearby mean motion resonance is 4J–2S–1 at $a \sim 2.41$ AU. Instead, we attribute this shape to dynamical evolution within the family (see above).

3.2. Massalia

Fig. 5 shows the number of asteroids associated with the Massalia family. The power-law exponent γ is given for the cumulative H distribution between (13.5, 15.5) as a function of the HCM velocity cut-off V_c . The critical values of V_c that bracket the family-defining interval are: (i) 34 m/s, where $a \leq 2.405$ AU asteroids merge with the family, and (ii) 47 m/s, where the cluster starts to accumulate a large portion of the surrounding main-belt population. In this case, we consider $V_c = 44$ m/s as a reasonable compromise to construct our nominal Massalia family.

The contrast between γ for the nominal family ($\gamma = 1.03 \pm 0.03$) and the overall background population is even larger than that for the Erigone family. A possible explanation for this is that the Massalia family was formed by a cratering rather than a catastrophic disruption event on a parent body with an estimated size of $D \sim 146$ –151 km (e.g., Tanga et al., 1999; Durda et al., 2006, in preparation). (20) Massalia’s large size (e.g., see Tedesco et al., 2002) means the mass ratio of Massalia to the parent object is large (~ 0.9 –0.99). The second largest object in this family, most likely the largest ejected fragment, is the Asteroid (7760) 1990 RW3; it is roughly $D \sim 7$ km.⁶ For asteroids at these sizes, the main-belt population should be in collisional equilibrium, such that the slope of its SFD is shallow.

Fig. 6 shows the nominal Massalia family. The distribution of proper eccentricity e and inclination I have been partly affected by weak resonances, notably the 4J–2S–1 and the exterior M1/2 mean motion resonance with Mars. The effect of the M1/2 resonance is prominently seen in the proper I of Massalia’s members at $a \sim 2.42$ AU. This does not mean, however, that the resonance does not also affect the proper e of these objects. In fact, we believe some Massalia members, by increasing or decreasing their proper e , may have become displaced enough to escape the family (see Section 5.2). As before, extreme values in a are, as in the Erigone case, “overpopulated” with small asteroids.

of the main-belt population near the Erigone family is in the range $H \sim 14$ –15 (Jedicke, R., private communication).

⁶ Note the larger associated object (2946) Muchachos is a recognized interloper in this family because it is spectrally inconsistent with (20) Massalia (Mothé-Diniz et al., 2005).

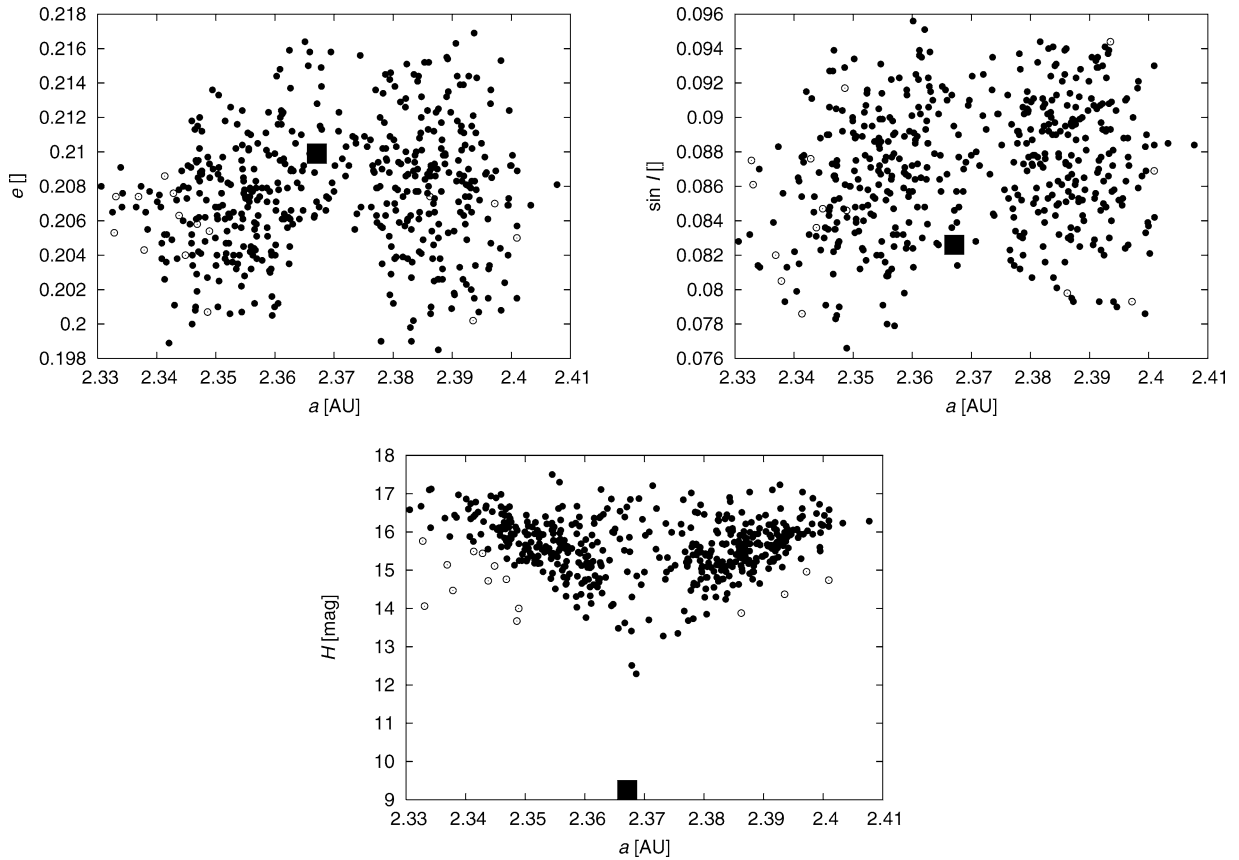


Fig. 4. Erigone family at HCM velocity 56 m/s projected onto a plane of proper semimajor axis a vs proper eccentricity e (top and left), proper semimajor axis a vs proper sine of inclination $\sin I$ (top and right), proper semimajor axis a vs absolute magnitude H (bottom); (163) Erigone is shown as a large filled square. Suspected interlopers are open circles. About half of these open circles at $a \leq 2.35$ AU is recognized alien to the family using the SDSS PC_1 – PC_2 clustering (Section 3.5).

3.3. Merxia

Fig. 7 shows the number of asteroids associated with the Merxia family as well as the local power-law exponent γ of the cumulative magnitude distribution in the (13.5, 15.5) range as a function of the HCM velocity cut-off V_c . As in the Masalia family case, there are two critical values of V_c : (i) 50 m/s, which brings both sides of the family together, and (ii) 108 m/s, where the family combines with the background main belt. Between these two values, the family stays “stationary” with few new asteroids connected to it. For this reason, our choice for the nominal family is $V_c = 80$ m/s. The SFD steepness parameter $\gamma = 0.63 \pm 0.03$ stays consistently larger than that corresponding to the local background population ($\gamma \sim 0.44$). Note that this family is located in the middle of the main belt (Fig. 2).

Fig. 8 shows the 3 characteristic projections of the Merxia family. An outstanding interloper in this family is (1327) Nannaqua; it has an X-type classification and a low geometric albedo that contrasts with the characteristic S-type classification in this family. Once again we see small members depleted from the central zone of the family (see below); this fits with our Yarkovsky/YORP evolution scenario. The family is intersected by the weak 3J–1S–1 three-body resonance, but limited leakage from the family is expected. It does produce, however, a dispersal in proper e and I for members drifting toward larger

a values (Section 5.3). The family is also bracketed by the J8/3 resonance at its low- a end.

3.4. Astrid

The Astrid family exhibits the simplest behavior of all 4 of the families examined here. As the HCM velocity cut-off V_c is increased (Fig. 9), the number of family members barely changes until 133 m/s, where a large portion of the middle and outer main-belt zone becomes linked to the family. Indeed, this family “lives in isolation” with its small proper I values (Fig. 2). Its only evolutionary obstacle is the prominent J5/2 mean motion resonance with Jupiter; this resonance may have prevented perturbed asteroids from reaching large a values.

A quick look at the (a, e) projection in Fig. 2, however, might cause one to adopt an incorrect conclusion, namely that the zone between the Astrid family and the J5/2 resonance is populated by a small but non-negligible number of asteroids. This is not true, however, because these objects have high inclinations. A closer look at a 3-dimensional section of the proper elements space near the Astrid family shows that the zone between the family and the J5/2 resonance is essentially empty. We find this feature unusual, so much so that in Section 5.4 we examine the formation of this feature using dynamical simulations. The fact that we are unable to come up with a plausible

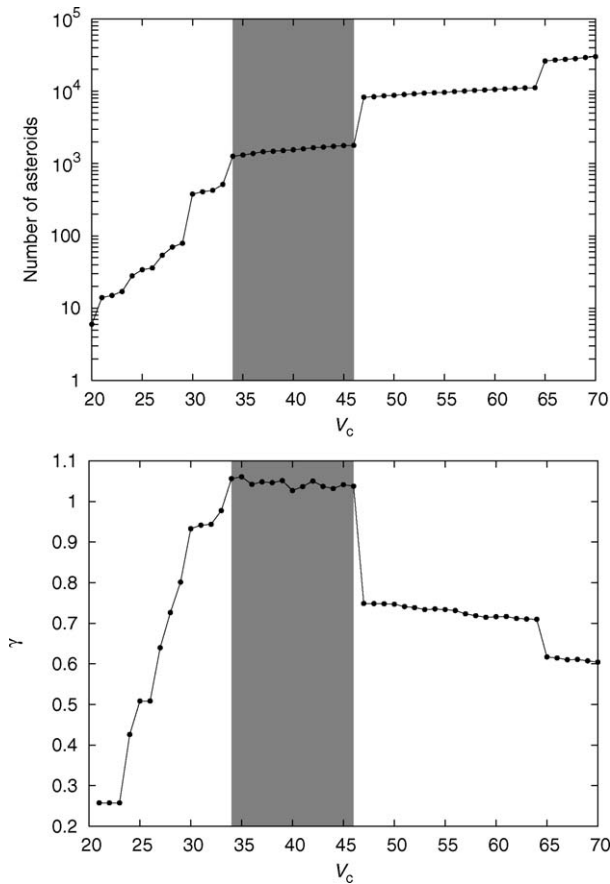


Fig. 5. The same as in Fig. 3 but for Massalia family. Critical transitions occur for $V_c = 47$ m/s, for which the family accumulates surrounding main-belt asteroids, and 64 m/s, when basically all inner main-belt asteroids coalesces with the family. The transition at $V_c = 34$ m/s has to do with associating all left side of the family (for which $a \leq 2.405$ AU) and only for that value the family is assumed to be complete. In between 34 and 46 m/s the number of the family members only slightly increases and its γ slope remains extremely high ($\simeq 1.03$).

solution for this population may suggest our model is missing some important feature or that the initial velocity field of the Astrid family was asymmetric. In such a case, Astrid may have predominantly populated orbits with a smaller than that of the largest body (1128) Astrid. We note the “left side of the family” ($a \leq 2.787$ AU) is well-determined and shows all attributes predicted by our model.

3.5. General issues

So far, our families have been characterized using proper element clustering techniques. To determine the sizes of the family members, however, we need to convert their H values to D . This relation depends upon their (unknown) geometric albedo p_V . To obtain, or at least constrain p_V , we use two sources of information.

First, we examine Tedesco et al. (2002), who reanalyzed the IRAS (Infrared Astronomical Satellite) database of infrared observations for moving objects. Geometric albedo p_V values were determined for 2228 individual objects. Among them, we searched for members of our nominal families. Unfortunately,

our families consist mainly of small asteroids that were not within the reach of IRAS observations. We obtained useful information mainly for Erigone and Merxia family members.

In the Erigone case, we identified 6 members among the Tedesco’s et al. catalog; all have albedos in the range 0.035–0.07, with a mean of 0.053. This value is a good fit to the average albedo found for C-type asteroids. Only 2 Merxia-family objects have known albedos: (808) Merxia, with $p_V = 0.22 \pm 0.04$, and (1327) Namaqua, with $p_V = 0.04 \pm 0.01$. The information suggests Namaqua is an interloper in the Merxia family. Indeed, its spectral classification X is discordant with the S-type asteroids in the Merxia family (Mothé-Diniz et al., 2005). The (a, H) position of this asteroid (Fig. 8) is also anomalous relative to the family’s configuration. For the Massalia family, we only have information on (20) Massalia ($p_V = 0.21 \pm 0.01$). Finally, for the Astrid family, we have (1128) Astrid with $p_V = 0.077 \pm 0.010$ and (2169) Taiwan with $p_V = 0.099 \pm 0.020$. In each of these cases, the values conform to the taxonomic type of the corresponding families.

As an additional source of information, we used a database provided by the Sloan Digital Sky Survey’s (SDSS) five color photometry (e.g., Ivezić et al., 2001; Jurić et al., 2002) to characterize the reflectance of smaller asteroids inside our families. We used the same methodology and data analysis described by Nesvorný et al. (2005), though we have taken advantage of an updated release of SDSS data. This source contains five color data about 43,424 individual moving objects that were positively identified with known sources. Searching this database, we found information on 104, 301, 83, and 20 asteroids in the Erigone, Massalia, Merxia, and Astrid families, respectively. For each of them, we constructed normalized reflectance spectra and computed their principal components PC_1 and PC_2 (see Eq. (1) in Nesvorný et al. (2005) and Roig and Gil-Hutton (2006), who derived numerical coefficients of the SDSS colors transformed into PC_1 and PC_2 for the third release catalogue). For our analysis, we only chose those objects with formal PC_1 and PC_2 errors smaller than 0.1. This translates into 35 objects in the Erigone family, 112 in the Massalia family, 44 in the Merxia family, and 7 in the Astrid family. In the Erigone family, we found 6 data-points significantly shifted from the remaining ones toward large values of PC_1 parameter; these would appear to be interloper S-type asteroids inside the family. Interestingly, this is consistent with our estimates as to which objects should be interlopers based on their orbital parameters (see the open circles in Fig. 4 for $a < 2.36$ AU).

Fig. 12 shows all these data projected onto the plane of principal components PC_1 and PC_2 ; our four families each are assigned different colors. Assuming membership in a family means the bodies have a similar mineralogy and hence a parametric relationship between PC_1 and PC_2 . We identify the families as distinct clusters in spectral parameter space in much the same manner as families are identified as clusters in proper element space. From the available data, and after we have eliminated several clear outliers, we can construct 90% confidence level zones for each families (see, e.g., Bertotti et al., 2003, Section 20.5). These are shown as the color-coded ellipses in Fig. 12. The approximate value $PC_1 \sim -0.08$ marks the di-

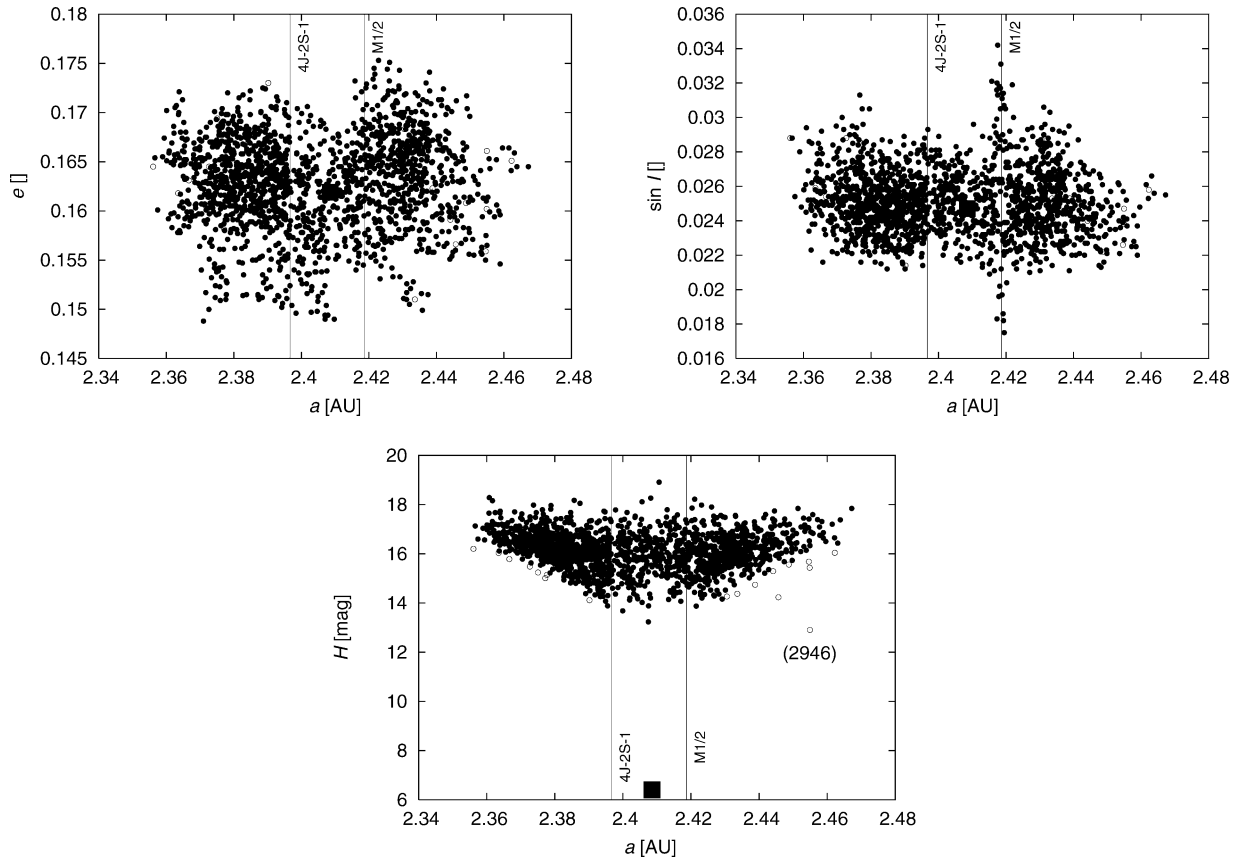


Fig. 6. Massalia family at HCM velocity 44 m/s projected onto a plane of proper semimajor axis a vs proper eccentricity e (top and left), proper semimajor axis a vs proper sine of inclination $\sin I$ (top and right), proper semimajor axis a vs absolute magnitude H (bottom); Asteroid (20) Massalia is shown as a large filled square. Suspected interlopers are open circles; Asteroid (2946) Muchachos is a spectrally confirmed interloper. Some of the weak mean motion resonances are shown: M1/2, an exterior resonance with Mars, produces the prominent spread of the inclination at $a \simeq 2.42$ AU, 4J–2S–1, a three-body resonance, may be responsible for the larger scatter of eccentricity below $a \simeq 2.41$ AU (Section 5.2 and Fig. 20).

vision between the S-complex (for which $PC_1 > -0.08$) and C-complex (for which $PC_1 < -0.08$; e.g., Bus and Binzel, 2002 or Nesvorný et al., 2005, with only a constant shift in definition of PC_1 values, see Roig and Gil-Hutton, 2006). Except for a small overlap, perhaps due to a few remaining interlopers, the 90% confidence levels of the Erigone and Astrid families lie well within the C-complex zone, while the Massalia and Merxia families reside in the S-complex zone. Indeed, the respective families were classified this way by Mothé-Diniz et al. (2005), who used a recent compilation of narrow-band spectroscopy databases SMASS and S3OS2.

The crosses in Fig. 12 show mean PC_1 and PC_2 values for each family and their standard errors. This information is interesting within the context of our work, because Jedicke et al. (2004) and Nesvorný et al. (2005) related these mean values to the age of a family as an expression of the degree of space weathering. According to their work, we expect the Massalia and Merxia families to have similar ages, differing perhaps by $\sim 50\%$ or less. On the other hand, the age of the Erigone family might be an order of magnitude larger than that of the Astrid family. Obviously, the PC_1 -age relation brought by Nesvorný et al. (2005) is empirical; fluctuations about the mean trend are to be expected. Moreover, these authors used an approximate means to derive family ages, while here we use more precise methods to compute ages for our 4 families.

4. Selected families: Best-fit models

After having characterized our target families, we are now ready to apply our Yarkovsky/YORP family evolution code in order to match the observed $\mathcal{D}(C)$ (or $N_{\text{obs}}(C)$) distribution described in Section 2. Its main features and parameters are as follows:

- The initial orbits of the family’s fragments in proper element space were based on a test velocity distribution. The velocity components V_R , V_T , and V_N along the radial, transverse, and normal directions with respect to the parent body’s orbit were given the same Gaussian distribution with standard deviation V_{SD} . We assumed $V_{SD} = V$ (5 km/ D), where V is a free parameter of the model (characteristic to the ejecta velocity field after self-gravity has acted to accumulate them with typical values believed to be several tens of meters per second) and V_{SD} is thus inversely proportional to size D (Nesvorný et al., 2002b, 2003; Durda et al., 2004). The fragments were set to same number and H values as that of the observed family. The absolute magnitude H was converted to D using standard methods and a constant geometric albedo p_V (e.g., p_V was frequently derived from IRAS observations; Tedesco et al., 2002). In general, these values are consistent with the spec-

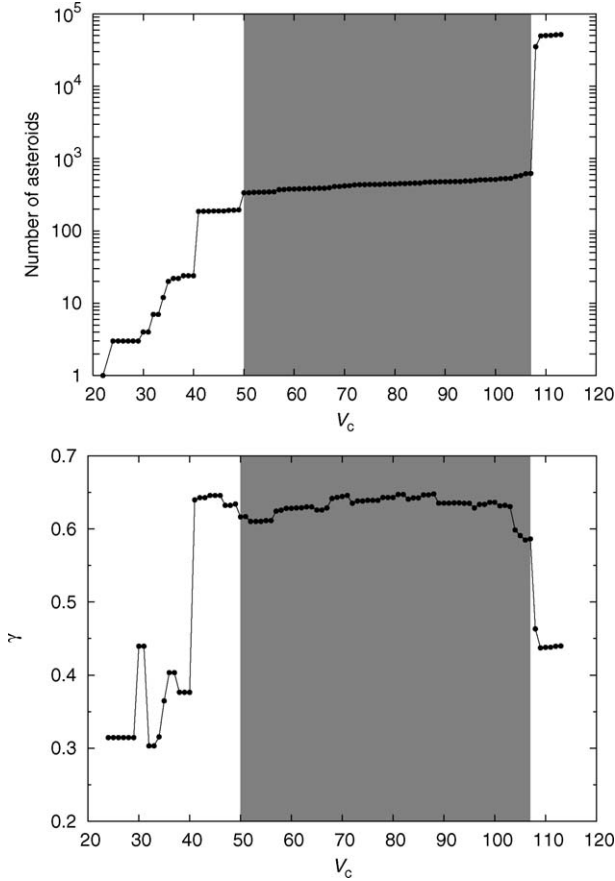


Fig. 7. The same as in Fig. 3 but for Merxia family. A critical transition occurs at $V_c = 108$ m/s, when the formal family coalesces with a fair portion of the middle and outer parts of the main asteroid belt. Two “internal” transitions occur at $V_c = 41$ m/s, when the whole left part of the family associates with the nearest surrounding of (808) Merxia, and at $V_c = 50$ m/s, when also the right part of the family (for which $a \geq 2.75$ AU) associates with the family. Until the coalescence with the bulk of asteroid belt, the family’s γ parameter is consistently high in between the 0.62 and 0.65 values.

tral type of the family. To test our solution, we vary p_V over different simulations.

- Apart from the size and initial orbital elements of each fragment (semimajor axis in particular), we also assigned an initial obliquity value ϵ and angular rotation velocity ω . The initial orientation of spin axes is random in space, allowing $\cos \epsilon$ to be uniformly distributed in the interval $(-1, 1)$.⁷ We assumed that ω had a Gaussian distribution peaked at $\simeq 6$ h. Values smaller than 2 h and longer than 12 h were rejected.
- The orbital evolution of each fragment was tracked individually, with Yarkovsky drift (e.g., Vokrouhlický, 1998, 1999)

$$\frac{da}{dt} = \kappa_1 \cos \epsilon + \kappa_2 \sin^2 \epsilon, \quad (8)$$

where κ_1 and κ_2 are functions depending on surface thermal parameters and the fragment’s size. We use the follow-

ing thermal parameters: thermal conductivity $K = 0.005 - 0.05$ W/m/K, specific heat capacity $C_p = 680$ J/kg/K, surface and bulk densities 2 and 2.5 g/cm³. Lower values of the thermal conductivity are preferred for S-type families and higher values for C-type families. To check the robustness of our solution, we change K over a limited interval of values. Equation (8) assumes (i) a spherical body residing on circular orbit about the Sun, and (ii) a restricted, linearized analysis of heat diffusion within the asteroid. We find these approximations reasonable because tests using a more complete numerical analysis show that Eq. (8) rarely fails by more than a factor of 2.

- The two rotation state parameters, obliquity ϵ and rotation rate ω , undergo evolution due to the YORP effect according to

$$\frac{d\omega}{dt} = f(\epsilon), \quad (9)$$

$$\frac{d\epsilon}{dt} = \frac{g(\epsilon)}{\omega} \quad (10)$$

(e.g., Vokrouhlický and Čapek, 2002; Čapek and Vokrouhlický, 2004). The f - and g -functions here are the median strength of the YORP torques derived by Čapek and Vokrouhlický (2004) for asteroids with surface thermal conductivity values within the range stated above. We caution, however, that our YORP model is less certain than our Yarkovsky effect model. For this reason, we introduce a free parameter c_{YORP} by which we multiply the f - and g -functions in Eqs. (9) and (10).

- Finally, we assume that non-catastrophic collisions can reorient the spin vectors of our test asteroids, which in turn modifies the Yarkovsky and YORP effects. Disruptive collisions are neglected. To implement this, we follow the approach developed by Farinella et al. (1998) and use the following formula to estimate spin axis re-orientation timescales:

$$\tau_{\text{reor}} = B(\omega/\omega_0)^{\beta_1} (D/D_0)^{\beta_2}, \quad (11)$$

with $B = 84.5$ kyr, $\beta_1 = 5/6$, and $\beta_2 = 4/3$. The reference size $D_0 = 2$ m and rotation frequency ω_0 correspond to a rotation period of 5 h. Propagating the family’s evolution over timesteps Δt (we typically take $\Delta t \sim 500$ yr), we compute for each timestep the probability $\sim \Delta t/\tau_{\text{reor}}$ that the spin vector would be collisionally reset to a new random state. We note, however, that for young families, collisional reorientation only plays a minor role. This was verified by excluding this effect, and re-running our model. No significant changes were seen in our results.

Once the initial configuration of the family has been determined, we run our code for a time T , ranging typically from 0 to 1 Gyr, and let the family evolve by thermal effects. As mentioned above, apart from T we consider 2 other free-to-fit parameters: V and c_{YORP} . To obtain a measure of the quantitative agreement between the simulated and the observed family,

⁷ We find this a useful starting point but see also Paolicchi (2005) for alternative possibilities.

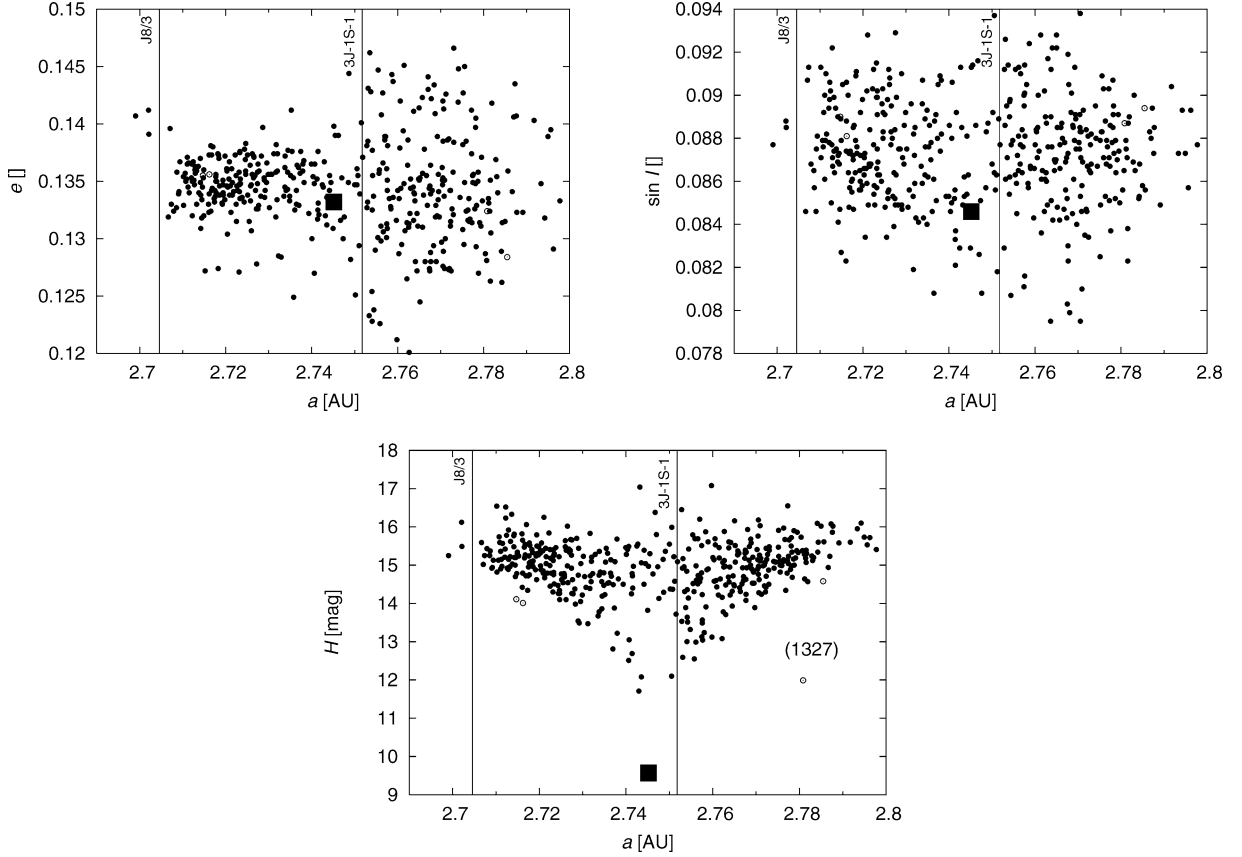


Fig. 8. Merxia family at HCM velocity 80 m/s projected onto a plane of proper semimajor axis a vs proper eccentricity e (top and left), proper semimajor axis a vs proper sine of inclination $\sin i$ (top and right), proper semimajor axis a vs absolute magnitude H (bottom); Asteroid (808) Merxia is shown as a large filled square. Suspected interlopers are open circles; Asteroid (1327) Namaqua is a spectrally recognized interloper. Some of the weak mean motion resonances are shown: 3J–1S–1, a three-body resonance, is likely responsible for the large scatter of proper eccentricities for $a \geq 2.75$ AU (Section 5.3 and Fig. 21).

we define a pseudo- χ^2 target function

$$\Psi_{\Delta C} = \sum_{\Delta C} \frac{[N(C) - N_{\text{obs}}(C)]^2}{N_{\text{obs}}(C)}, \quad (12)$$

where formally the error assigned to the number $N_{\text{obs}}(C)$ in a given bin $(C, C + \Delta C)$ is $\sqrt{N_{\text{obs}}(C)}$. Our procedure seeks to minimize $\Psi_{\Delta C}$ via variations of the 3 parameters over our chosen interval of values. Admissible solutions are characterized by $\Psi_{\Delta C}$ of the order equal to the number of used bins in C , while solutions giving much larger $\Psi_{\Delta C}$ are incompatible with the observed family. We use the incomplete gamma function $Q(a, \Psi_{\Delta C}^*)$ as a goodness-of-fit parameter (see, e.g., Press et al., 1999), where a is the number of ΔC -bins minus three (number of free parameters) and $\Psi_{\Delta C}^*$ is the minimum value of the target function (12). In general, $Q \sim 1$ characterize a very good fit while a small value of Q means a poor fit. Since our result always yield a high-quality fit ($Q \geq 0.98$), we simplify the parameter-error analysis by deriving them from the level curve of $\Psi_{\Delta C} = a + 3$, i.e., level curve of the target function equal to the number of ΔC -bins (“observations”). Solution of this $\Psi_{\Delta C}$ level-curve corresponds to $Q \sim 0.2$ – 0.3 .

We also note that in all solutions presented in this paper, we use the current luminosity L of the Sun. Evolutionary models of the solar interior imply the Sun should have been about 25% fainter some 4 Gyr ago (e.g., Bahcall et al., 2001, Ta-

ble II). A smaller radiation flux in the past should produce weaker thermal effects in the Yarkovsky and YORP effects. An investigation of this effect on the Eos family, however, showed it only changed the family age by $\sim 4\%$ (Vokrouhlický et al., 2005). For this reason, and because the families studied here are ≤ 1 Gyr old, we ignore the effects of variable L in this paper.

4.1. Erigone

Fig. 13 shows the contour plots of $\Psi_{\Delta C}$ projected onto 2-D parameter planes T vs c_{YORP} , T vs V , and c_{YORP} vs V . The best-fit solution for $N(C)$, together with the observed data $N_{\text{obs}}(C)$ and their formal error-bars, is shown in the same figure (left and top). For our first set of runs, we assume a constant geometric albedo $p_V = 0.05$ and thermal conductivity $K = 0.05$ W/m/K for all asteroids. For the contour plots, we chose the best $\Psi_{\Delta C}$ -value along the suppressed dimension. The minimum value of the target function found is $\Psi_{\Delta C}^* = 7.3$; considering the number of degrees of freedom equal to 18 we obtain $Q \simeq 0.987$ of the best-fit solution. The “critical” isoline value of $\Psi_{\Delta C} = 21$ is plotted in bold (recall this value formally corresponds to solutions that barely match the observed family at the chosen σ -interval from all data points and is used to give us some idea of the uncertainty of the solved-for param-

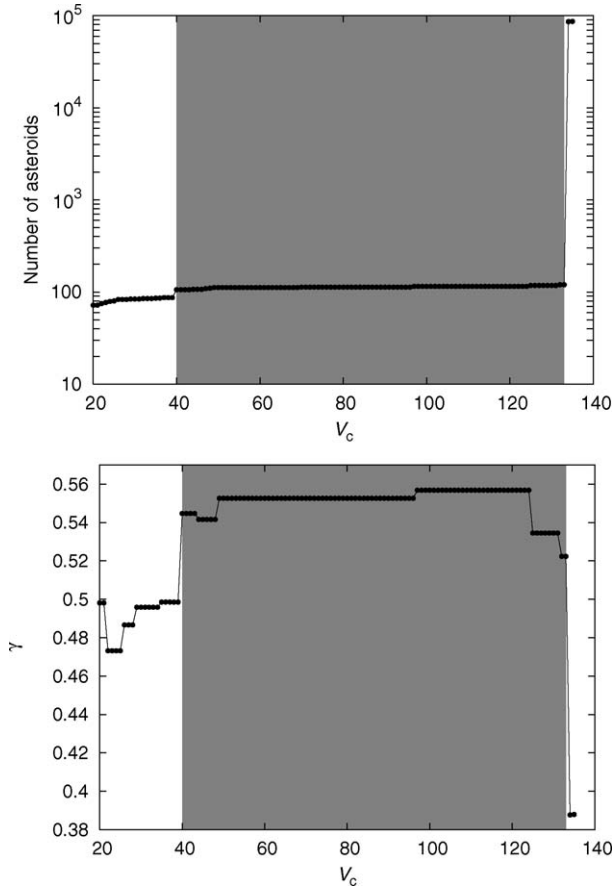


Fig. 9. The same as in Fig. 3 but for Astrid family. The family shows only a weak dependence on the HCM velocity cut-off V_c at the abscissa until a critical value of 133 m/s, when the family coalesces with the surrounding zone of the main belt.

ters). If this threshold parameter is reasonable, the best solution for the three parameters is: $T = 340^{+60}_{-40}$ Myr, $c_{\text{YORP}} = 0.8^{+1.2}_{-0.5}$, and $V = 32^{+8}_{-17}$ m/s. Note that the 3 parameters are correlated, such that a stronger YORP effect (c_{YORP}) pushes the family age (T) to smaller values. We also find that the strength of the YORP effect is weakly constrained, but that some YORP effect is needed to produce the displaced maximum in $N_{\text{obs}}(C)$. The best-fit velocity V is low but compatible with the expected values from hydrocode modeling (e.g., Durda et al., 2004). From the best-fit solution we infer, therefore, that the family once had a span in semimajor axis roughly half of that the observed one.

Next, we tested the robustness of our solution with regards to changes in the surface thermal conductivity K . We chose a number of random values of K between 0.005 and 0.05 W/m/K. Our new best-fit solution was $T = 280^{+30}_{-50}$ Myr, $c_{\text{YORP}} = 0.6^{+1.4}_{-0.2}$, and $V = 26^{+14}_{-11}$ m/s. The minimum target function value was $\Psi_{\Delta C}^* = 6.8$, rendering the fit little better than before. While the solutions for V and c_{YORP} parameters did not change very much, the estimated age of the family T shifted to a smaller value. The same would occur if we assumed a larger mean value for the family members' geometric albedo p_V . Our experiments show that $T \propto p_V^{-a}$, where $a \sim 0.5$. This approximate scaling law would be expected if the Yarkovsky/YORP effects play a significant role in determining the current fam-

ily distribution; recall that the strength of the Yarkovsky forces are inversely proportional to the size of the bodies. The above relation is, however, approximate and may also depend on the nature of the chosen family, its initial velocity distribution, and the speed of Yarkovsky/YORP evolution.

We believe the mean albedo is unlikely to be significantly smaller than ~ 0.05 , such that 400 Myr represents an approximate upper limit for the age of this family. With $p_V \sim 0.1$ and our lowest assumed thermal conductivity of 0.005 W/m/K, we obtain an age of 160^{+30}_{-30} Myr for Erigone. Given that we do not have solid values for the geometric albedo, and to a lesser extent surface thermal conductivity, this is the best we can do with the available data. Hence, we conclude that the age of Erigone is ~ 280 Myr with an uncertainty of $\sim 40\%$. Previous tests indicate that better determined values of mean p_V and K values would allow us to reduce the uncertainty in the age to the $\sim 10\%$ level. The same caveat applies to the solutions for the other families discussed below.

4.2. Massalia

Fig. 14 shows the distribution $N_{\text{obs}}(C)$ of the Massalia members in the C -parameter from Eq. (2) ($\beta = 1$) with errors bars $\sqrt{N_{\text{obs}}(C)}$. Unlike the Erigone case, here we observe an asymmetry about $C = 0$ such that the peak at negative C values is larger than at positive C values. Figs. 2 and 6 show why this happens: the family is cut by a weak exterior mean motion resonance with Mars (M1/2) that likely caused some family member to escape the family cluster. The fraction of objects removed from the family is unknown. For that reason, we decided to discard the $C > 0$ data and instead concentrate on fitting the $C < 0$ distribution.

Fig. 15 shows our solution for $p_V = 0.21$ (as inferred for Massalia family members) and surface thermal conductivity $K = 0.005$ W/m/K. The best-fit solution minimizes the target function (12) to $\Psi_{\Delta C}^* = 9.3$ ($Q = 0.987$); here the critical level curve is 24 (i.e., number of data points). The solved-for parameters have the following values: $T = 152^{+18}_{-18}$ Myr, $c_{\text{YORP}} = 0.2^{+1.8}_{-0.1}$, and $V = 17^{+5}_{-5}$ m/s. Except for $c_{\text{YORP}} \sim 0$, which is excluded, our match to the Massalia family only weakly constrains the strength of the YORP effect. On the other hand, the family age T and the velocity parameter V are surprisingly well constrained. This solution nearly does not change if K is allowed to span an interval between 0.001 to 0.01 W/m/K. Should the Massalia family have an anomalously large p_V value (e.g., $p_V \sim 0.12$), we obtain the following best-fit parameter values: $T = 190^{+40}_{-20}$ Myr, $c_{\text{YORP}} = 0.5^{+1.5}_{-0.3}$, and $V = 25^{+5}_{-8}$ m/s. We thus conclude that the upper limit for the Massalia family's age is ~ 240 Myr, but that a more likely age is ~ 150 – 200 Myr.

The diameter of largest asteroid in the Massalia family, called (20) Massalia, is $D \approx 145$ km (Tedesco et al., 2002). Durda et al. (2006, in preparation) estimate it represents nearly 99% of the family parent object mass (slightly more than Tanga et al. (1999) who give 90%). This means the Massalia family is a byproduct of a cratering event. This may produce a lower velocity dispersion parameter V than that for the Erigone family,

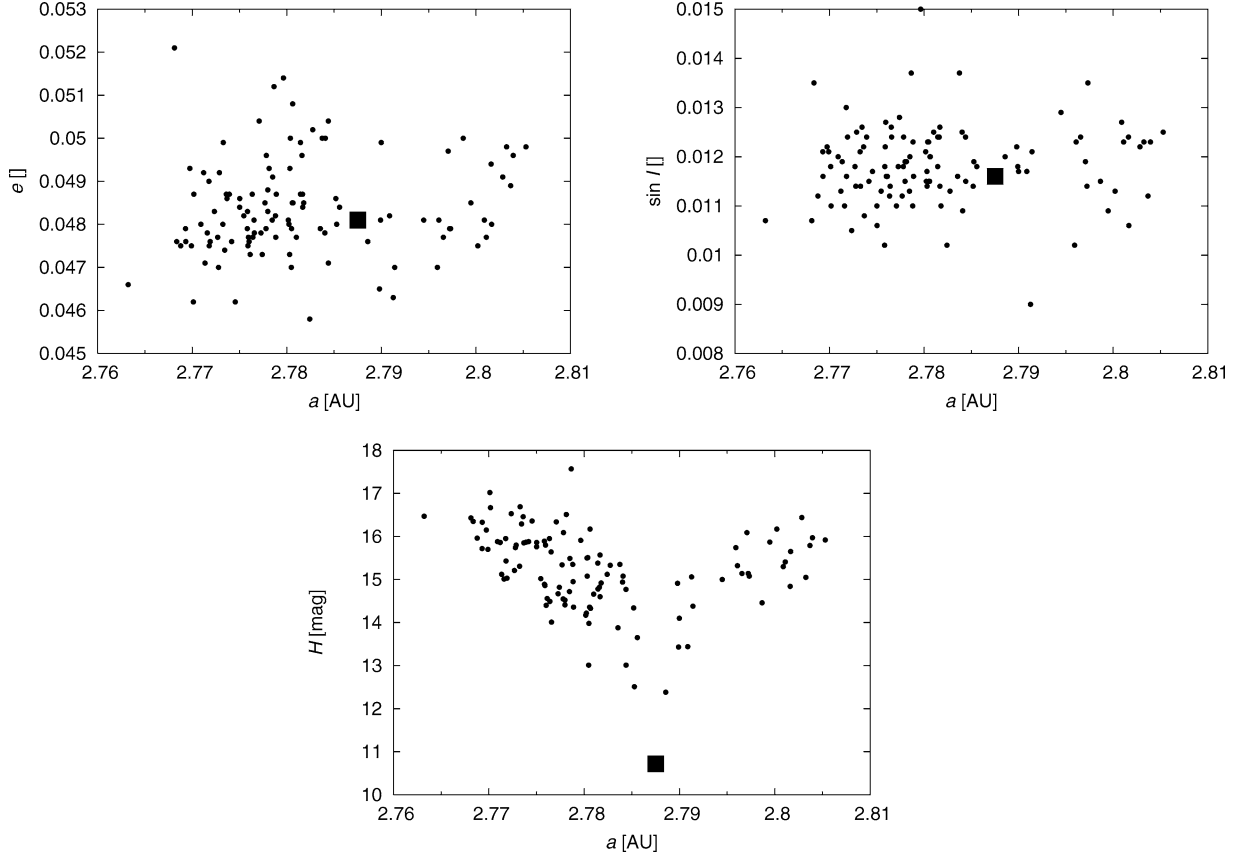


Fig. 10. Astrid family at HCM velocity 70 m/s projected onto a plane of proper semimajor axis a vs proper eccentricity e (top and left), proper semimajor axis a vs proper sine of inclination $\sin I$ (top and right), proper semimajor axis a vs absolute magnitude H (bottom); (1128) Astrid is shown as a filled square.

whose parent body was only $D \sim 110$ km. On the other hand, the Massalia family is dominated by $D \simeq 1\text{--}2$ km asteroids, for which our solution leads to dispersal velocities comparable to (20) Massalia’s escape velocity ($\simeq 85$ m/s). This is in good agreement with expectations from cratering events (e.g., compare with results for the Vesta family; [Asphaug, 1997](#)).

Analysis of the Massalia family’s age is of particular interest because it has been proposed as a possible source (along with the Themis family) for the α dust band (e.g., [Nesvorný et al., 2003](#)). While the Massalia family is much smaller than that of Themis, it is also much younger. Thus, it is unclear which one should dominate dust production. We leave an investigation of this issue to future work.

4.3. Merxia

Like the Erigone family, the Merxia family exhibits a symmetric $N_{\text{obs}}(C)$ distribution, enough that negative and positive C values can be folded together into bins without a loss of information ([Fig. 16](#); upper and left panel). The other panels of the figure show our solutions for $p_V = 0.22$ (as inferred for (808) Merxia) and $K = 0.005$ W/m/K. The best-fit solution minimizes the target function (12) to $\Psi_{\Delta C}^* = 3.9$ ($Q = 0.996$), to be compared to the critical-level value of 17 (number of data points). The solved-for parameters have the following values: $T = 238_{-23}^{+52}$ Myr, $c_{\text{YORP}} = 0.6_{-0.4}^{+1.4}$, and $V = 24_{-12}^{+6}$ m/s. The overall character of the solution is similar to those described

above. For instance, it is robust against changes to K . Assuming values between 0.001 to 0.01 W/m/K, we find best-fit values that only have slight changes. In a less probable case, where all small members of the Merxia family have systematically smaller p_V values (e.g., $p_V \sim 0.12$), the best-fit age of the family becomes $T = 325_{-50}^{+75}$ Myr. Thus, the maximum age for the Merxia family is $\lesssim 400$ Myr.

Overall, our solutions are consistent with estimates suggesting that the Massalia family is $\sim 50\%$ younger than the Merxia family (Section 3).

4.4. Astrid

[Fig. 17](#) shows the $N_{\text{obs}}(C)$ distribution for the Astrid family. Here the asymmetry is even more pronounced about the $C = 0$ value than in the Massalia case ([Fig. 14](#)). The reason is that the portion of the family with $a \geq 2.787$ AU is significantly underpopulated ([Fig. 10](#)). In Section 5.4, we discuss our search for a putative dynamical mechanism to deplete the zone between the Astrid family and the J5/2 mean motion resonance (though we note here that we failed to find any). We cannot rule out the possibility that the family had an initially anisotropic velocity field or an unequal initial distribution of spin axis obliquities, but we do not find either explanation very satisfying. We tentatively use the $a \leq 2.787$ AU portion of the family in our analysis (thus $\mathcal{D}(C)$ with $C < 0$), but we are aware that these results are the least certain in our paper.

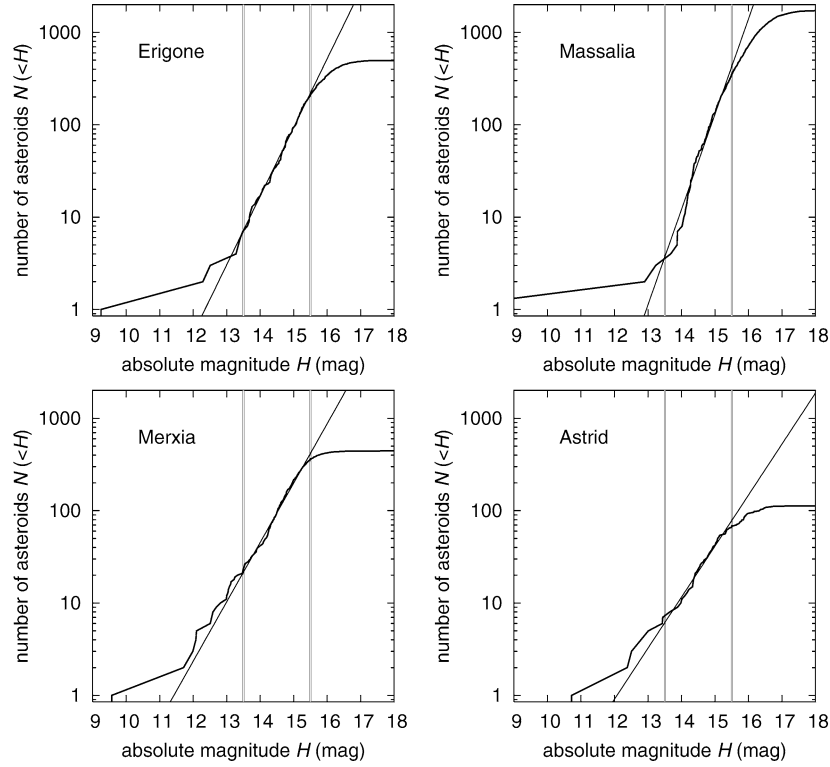


Fig. 11. The cumulative distributions $N(<H)$ for: (i) Erigone (top and left), (ii) Massalia (top and right), (iii) Merxia (bottom and left), and (iv) Astrid (bottom and right); nominal families shown here. We use $N(<H) \propto 10^{\gamma H}$ approximation in the magnitude range (13.5, 15.5) and obtain the following values of the γ parameter: (i) $\gamma = 0.74$ for Erigone, (ii) $\gamma = 1.03$ for Massalia, (iii) $\gamma = 0.64$ for Merxia, and (iv) $\gamma = 0.55$ for Astrid. The exponent β of the power-law approximation of the cumulative size distribution is related to γ as $\beta = -5\gamma$. Except for the Astrid family, the magnitude distribution is much steeper than the collisionally evolved system for which *Dohnanyi (1969)* derived $\gamma_{\text{Doh}} = 0.5$ or $\beta_{\text{Doh}} = -2.5$.

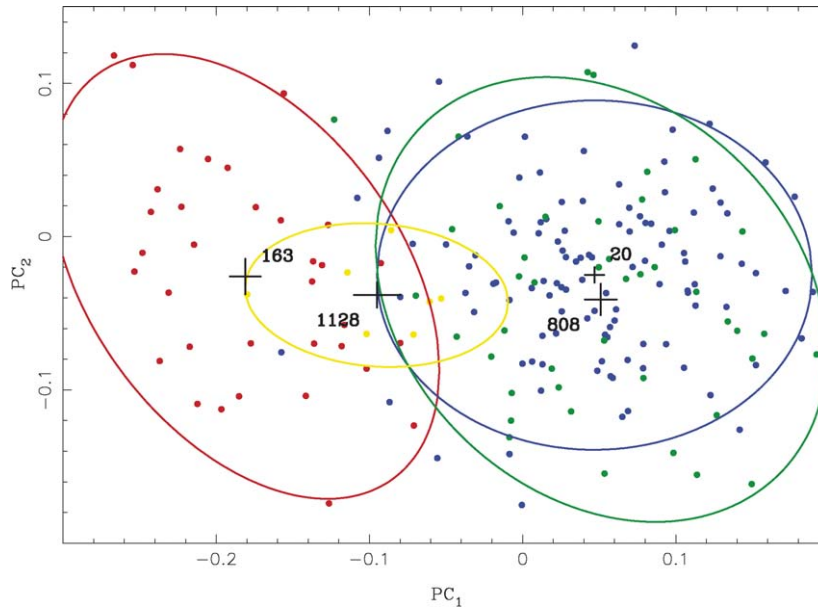


Fig. 12. Principal spectral components PC_1 and PC_2 derived for members of our studied families from the Sloan Sky Digital Survey (SDSS; data release 3 and the PC_1 and PC_2 values computed as in *Roig and Gil-Hutton, 2006*). Dots are data for individual asteroids: Erigone members (red), Astrid members (yellow), Massalia members (blue), and Merxia members (green). The black crosses are mean values in the corresponding family with standard errors; labels are the number of leading asteroid in the family, thus (163) Erigone, (1128) Astrid, (20) Massalia, and (808) Merxia. The ellipses show 90% confidence level boundaries of membership for each of the families based on the available SDSS data.

Fig. 18 shows our solution for $p_V = 0.08$, with $K = 0.05$ W/m/K uniformly assigned to all Astrid members. The

best-fit solution minimizes the target (12) to $\Psi_{\Delta C} = 1.3$ ($Q = 0.995$); this value should be compared with the critical-level

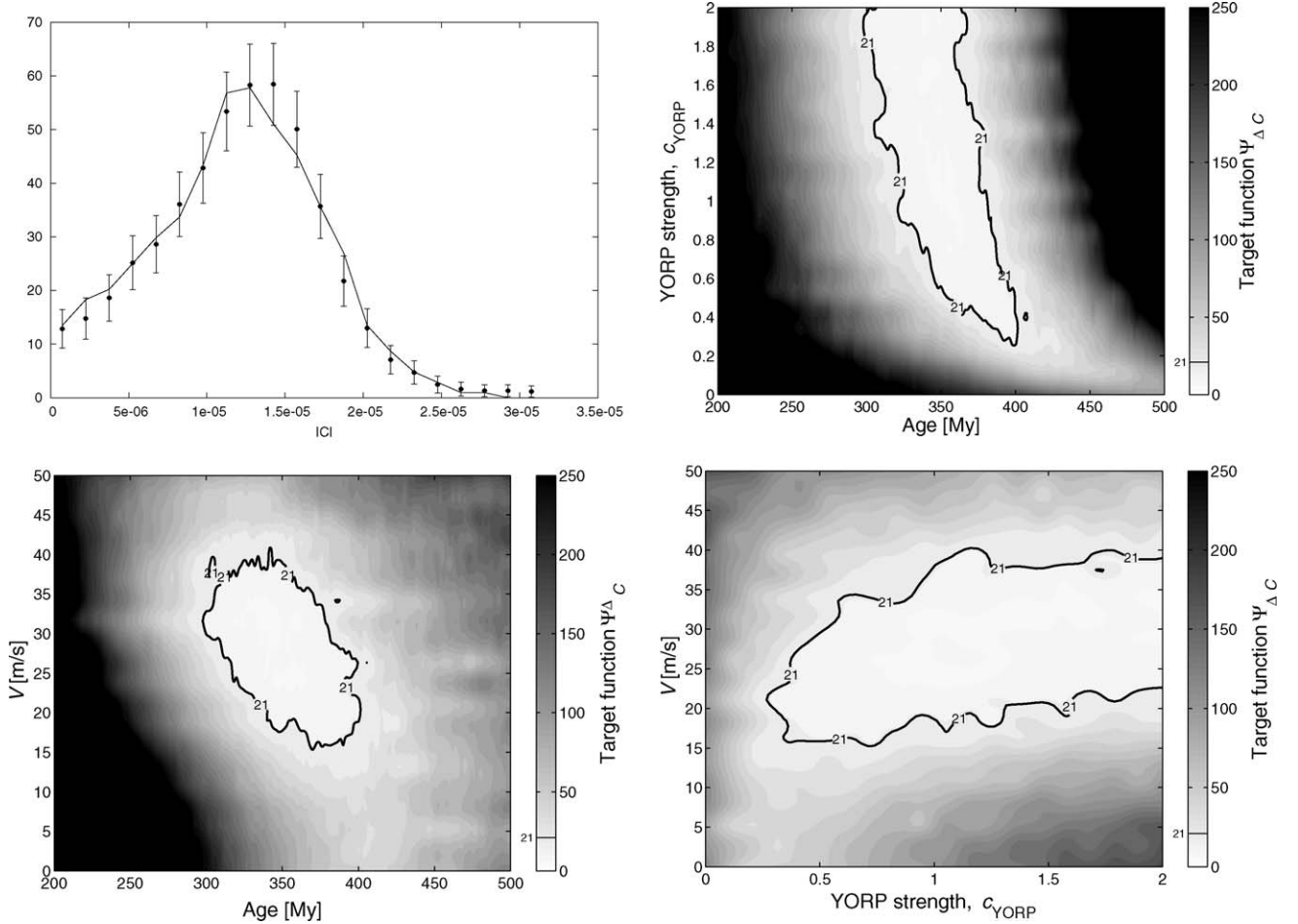


Fig. 13. Results of our simulation for the Erigone family with mean albedo $p_V = 0.05$ and surface thermal conductivity $K = 0.05$ W/m/K. The best-fit solution $N(C)$ (solid line) over-imposed over data points $N_{\text{obs}}(C)$ (intervals)—top and left; $N(C)$ is symmetric about $C > 0$ and in our analysis we folded asteroids with $C < 0$ into the corresponding bin with $C > 0$. Top and right, and bottom figures show projection of the best value of the target function $\Psi_{\Delta C}$ for various pairs of the solved-for parameters: (i) age T vs YORP strength parameter c_{YORP} , (ii) age T vs characteristic velocity V of initial ejection of $D = 5$ km fragments, and (iii) c_{YORP} vs V . The critical-level contour $\Psi_{\Delta C} = a + 3 = 21$, a is the number of degrees of freedom, that serves to estimate uncertainties of the solved-for parameters is shown in bold; other values of the target function are shown in scales of gray.

value of 11 (number of data points). The solved-for parameters have the following values: $T = 214^{+116}_{-44}$ Myr, $c_{YORP} = 0.9^{+1.1}_{-0.9}$, and $V = 13^{+12}_{-13}$ m/s. Here our solution is the poorest among all of the cases discussed in this paper, possibly because the number of available asteroids used as constraints was small. The characteristic ejection velocity V of the $D \sim 5$ km fragments is smaller than in the Merxia and Erigone cases. This may be due to the fact that the parent body of the Astrid family was only $D \sim 60\text{--}70$ km (Durda et al., 2006, in preparation). Using K values between 0.005 to 0.05 W/m/K, we find the age becomes $T = 180^{+80}_{-40}$ Myr. Further decreases occur if mean geometric albedo is higher than 0.08. This possibility, however, does not seem likely for a C-type family.

If the initial velocity field was anisotropic, such that the a distribution of the family was skewed toward $a < a_c = 2.787$ AU, our result would overestimate the family's age. A factor 2 is not excluded, so that the Astrid family may be as young as ~ 100 Myr (e.g., Nesvorný et al., 2005).

5. Selected families: Additional simulations

In this section we complement, and in some cases strengthen, our Yarkovsky dispersion model for chosen families by tracking the evolution of a limited number of family asteroids using numerical integration. We believe these results may explain some of the more peculiar features noted above.

We use a SWIFT-RMVS integrator (e.g., Levison and Duncan, 1994) modified to account for the Yarkovsky forces and with a second order symplectic map due to Laskar and Robutel (2001) (see <http://sirrah.troja.mff.cuni.cz/yarko-site/> for details of the implementation, rapidity and accuracy tests). We also complemented the original version of the integrator with an on-line computation of synthetic proper elements in a manner compatible with a definition from Knežević and Milani (2000, 2003). This means we first apply a Fourier filter to the (non-singular) orbital elements in a moving window of $\simeq 0.7$ Myr (with steps of 0.1 Myr) to eliminate all periods smaller than some threshold (1.5 kyr in our case). The filtered signal is output from the simulation for further checks

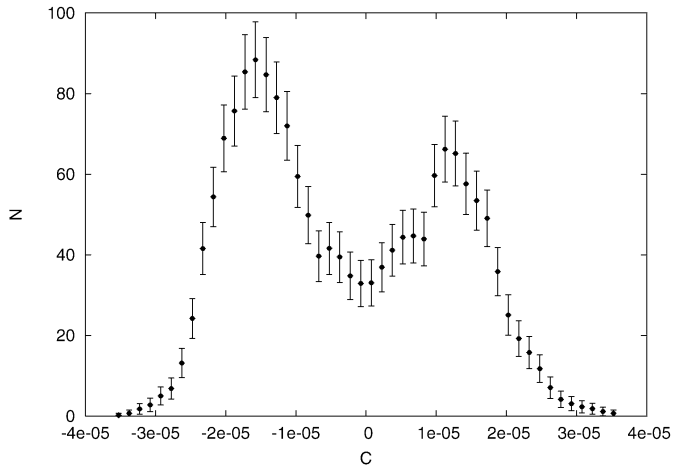


Fig. 14. Symbols show number $N_{\text{obs}}(C)$ of observed Massalia members in $(C, C + \Delta C)$ bins with error-bars given as $\sqrt{N_{\text{obs}}(C)}$. We chose $\Delta C = 1.5 \times 10^{-6}$ AU and a_c uniformly averaged in the range (2.407, 2.414) AU. In this case, $N(C)$ is not symmetric about $C = 0$, but the number of asteroids for positive C is systematically smaller. We suggest this is an effect of partial leakage of objects from the family along the exterior martian resonance M1/2. We thus decided to discard $C > 0$ distribution from our analysis and use only $N(C)$ for $C < 0$.

and passed through a frequency analysis code adapted from Šidlichovský and Nesvorný (1997) to obtain (planetary) forced and free terms in Fourier representation of the orbital elements. The isolated free terms are what we use as the proper orbital elements.

In the case of the inner main-belt families Erigone and Massalia, all planets except for Mercury and Pluto are included in our simulation. Their masses, initial positions, and velocities were taken from the JPL DE405 ephemerides. A timestep of 0.05 yr is used. For central main belt families Merxia and Astrid, we only included the outer planets in our simulation and used an integration timestep of 0.25 yr. To determine the initial orbital conditions for our test bodies, we selected a limited number of real asteroids from the corresponding family. We also used a number of fictitious objects (clones) whose orbital elements were created by making tiny (a, e) changes in the orbital parameters of real objects.

For each simulation, we typically integrated 100–200 test bodies for several hundred Myr. When Yarkovsky forces were included in the simulation, we assumed the bodies had sizes ranging between $D = 2$ –20 km. Rotation rates were assumed Maxwellian with a peak value corresponding to a period of 8 h (though we prevented shorter/longer periods than 4/12 h). In the Massalia, Merxia, and Astrid cases, we purposely wanted the bodies to migrate toward larger a values. For this reason, we set their obliquities $\simeq 45^\circ$; this underestimates the maximum possible drift rate by the diurnal variant of the Yarkovsky effect by a factor of $\simeq \sqrt{2}$. Thermal parameters, needed to model the Yarkovsky forces, are: $K = 0.005$ W/m/K, $C_p = 680$ J/kg/K, and surface and bulk densities 1.5 and 2.5 g/cm³. Small changes in these values do not modify our conclusions. We used the analytic formulae described in Vokrouhlický (1998, 1999) and Vokrouhlický and Farinella (1999, Appendix) for both diurnal and seasonal variants of the Yarkovsky effect.

5.1. Erigone

The purpose of our Erigone simulation was to determine whether the remarkable depletion in the center of the family (Fig. 4), interpreted above as a byproduct of Yarkovsky/YORP evolution, might have some alternative explanation. For example, could objects near the center have been affected by weak mean motion resonances? We investigate this scenario here using numerical integration, even though Nesvorný and Morbidelli (1998) suggest there are no meaningful resonances near the center of this family.

For these tests, we only include gravitational interactions. We selected 108 asteroids and their close clones in the central zone of the family and propagated their orbits forward 500 Myr into the future. Fig. 19 shows the resulting evolutionary tracks projected onto planes of proper a vs proper e and proper a vs proper sine of inclination $\sin I$. In some cases, the evolution tracks stay very near the initial point, indicating a very high degree of stability in this particular region. At the high- e end of the family, the synthetic proper elements indicate larger but stable oscillations. They are triggered by an interaction with the high-order secular resonance $z_2 = 2(g - g_6) + s - s_6$ (e.g., Milani and Knežević, 1992, 1994). In fact, we hypothesize that the upper bound is systematically lower in proper e for $a \leq a_c \simeq 2.37$ AU is produced by the z_2 resonance that efficiently captures Yarkovsky-moving asteroids (see the similar role of the z_1 resonance in the Eos family; Vokrouhlický et al., 2005). Without Yarkovsky/YORP evolution, however, this resonant effect is minimal. As a result, none of the objects in our sample evolved enough to escape from the family. This suggests that the central depletion must have formed by some other process.

5.2. Massalia

In Section 3.2 we noted that the Massalia family has been clearly affected by the exterior mean motions resonance M1/2 with Mars located at $a \simeq 2.42$ AU. A stream of asteroids is seen “radiating” from the family along this resonance in inclination space (Fig. 6). In Section 4.2 we determined that the $N_{\text{obs}}(C)$ distribution is markedly asymmetric about $C = 0$ with lower peak value for positive C (thus $a > a_c \simeq 2.407$ AU). We associated this asymmetry with the previously noted leakage through the M1/2 resonance. For that reason, we decided to only use the $C < 0$ values of the $N_{\text{obs}}(C)$ distribution that were unaffected by this resonance. In this section, we investigate whether the observed orbital structure of the Massalia family is compatible with these ideas within our Yarkovsky evolution model.

We selected 137 Massalia members in its central zone. The orbits of these bodies were numerically propagated for 240 Myr, the approximate age of the family (Section 4.2). The bodies were given a range of sizes $D = 0.7$ –9 km and the rotational and thermal parameters described above.

Fig. 20 shows the result of our experiment. The orbital tracks shown in this figure use double coding: (i) black—where the body is still associated with the real Merxia family with HCM cut-off velocity $V_c = 44$ m/s (corresponding to our nominal

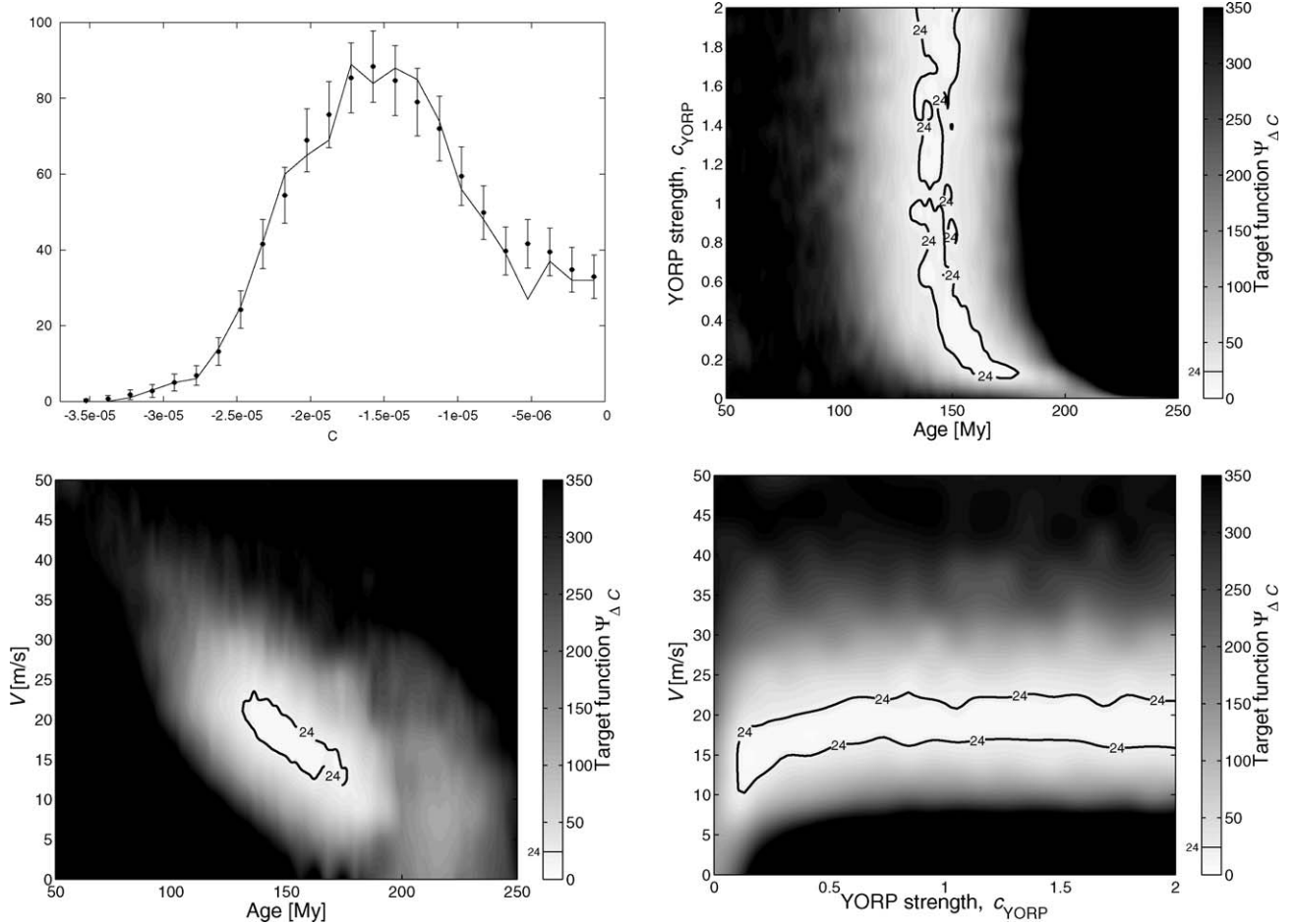


Fig. 15. Results of our simulation for the Massalia family with mean albedo $p_V = 0.21$ and surface thermal conductivity $K = 0.005$ W/m/K. Top and left is the best-fit simulation of number of asteroids $N(C)$ in the C -bins (solid line) compared to the observed family $N_{\text{obs}}(C)$ (symbols and error-bars). Top and right, and bottom figures show projection of the best value of the target function $\Psi_{\Delta C}$ for various pairs of the solved-for parameters: (i) age T vs YORP strength parameter c_{YORP} , (ii) age T vs characteristic velocity V of initial ejection of $D = 5$ km fragments, and (iii) c_{YORP} vs V . The critical-level contour $\Psi_{\Delta C} = a + 3 = 24$, a is the number of degrees of freedom, that serves to estimate uncertainties of the solved-for parameters is shown in bold; other values of the target function are shown in scales of gray.

family) and (ii) gray—where the orbital parameters are changed enough that the minimum HCM distance to any family members exceeds $V_c = 44$ m/s. The later shows the fate of those bodies escaping from the nominal family. We confirm that upon reaching the M1/2 resonance, some orbits get dispersed so that they cease to be identified as family members. In our runs, this happened to 22 objects of the 136 cases (16%). This may partly explain the asymmetry of the $N_{\text{obs}}(C)$ distribution from Fig. 14. As time proceeds, some of the family members fall into the J3/1 mean motion resonance at $a \simeq 2.48$ AU. The observed family is apparently on the brink of that situation.

5.3. Merxia

In this case, our goal is to understand the dispersion of the family members' proper e and, to a lesser extent, proper I values beyond the three-body resonance 3J–1S–1 ($a \simeq 2.75$ AU; Figs. 2 and 8). Our working hypothesis is that majority of members initially landed below this resonance (i.e., had $a < 2.75$ AU) and some migrated toward larger a -values by the Yarkovsky forces. Upon reaching this resonance, they might

have temporarily interacted with it, sliding toward both smaller and larger e and I values. When these bodies leave the 3J–1S–1 resonance, their e - and I -distributions would freeze-in information about this resonant interaction.

Fig. 21 shows the evolution of 145 orbits over 250 Myr, a timespan compatible with our best estimate of this family's age. Our starting data are several real asteroids associated with the family residing near its center, each of which has been cloned by making small changes to their orbital a and e values. Our test bodies had sizes in the range $D = 1.5$ –20 km, with rotational and thermal parameters as stated above. We again use the black/gray coding for segments of the evolutionary track that are (or are not) associated with the nominal family.

Our results indicate that 34 out of 127 drifting orbits that encountered the 3J–1S–1 resonance were eliminated from the family (27%). An important result is that the eccentricity and inclination dispersion becomes significantly larger and more compatible with the observed family members beyond the 3J–1S–1 resonance. This confirms our hypothesis and strongly supports our model of Yarkovsky/YORP dispersion. Surprisingly, the $N_{\text{obs}}(C)$ distribution of the Merxia family is nearly sym-

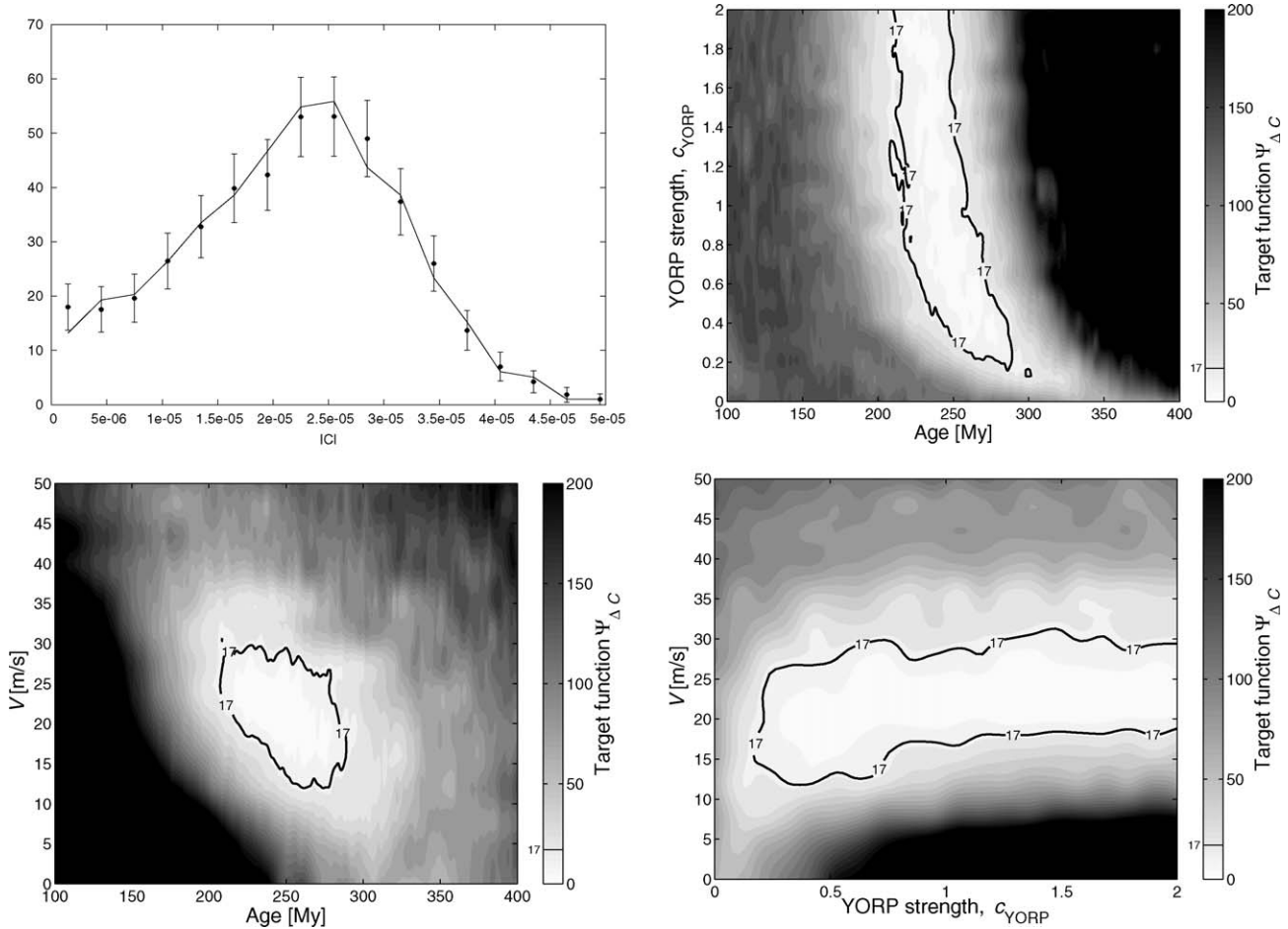


Fig. 16. Results of our simulation for the Merxia family with mean albedo $p_V = 0.22$ and surface thermal conductivity $K = 0.005$ W/m/K. Top and left is the best-fit simulation of number of asteroids $N(C)$ in the C -bins (solid line) compared to the observed family $N_{\text{obs}}(C)$ (symbols and error-bars). Top and right, and bottom figures show projection of the best value of the target function $\Psi_{\Delta C}$ for various pairs of the solved-for parameters: (i) age T vs YORP strength parameter c_{YORP} , (ii) age T vs characteristic velocity V of initial ejection of $D = 5$ km fragments, and (iii) c_{YORP} vs V . The critical-level contour $\Psi_{\Delta C} = a + 3 = 17$, a is the number of degrees of freedom, that serves to estimate uncertainties of the solved-for parameters is shown in bold; other values of the target function are shown in scales of gray.

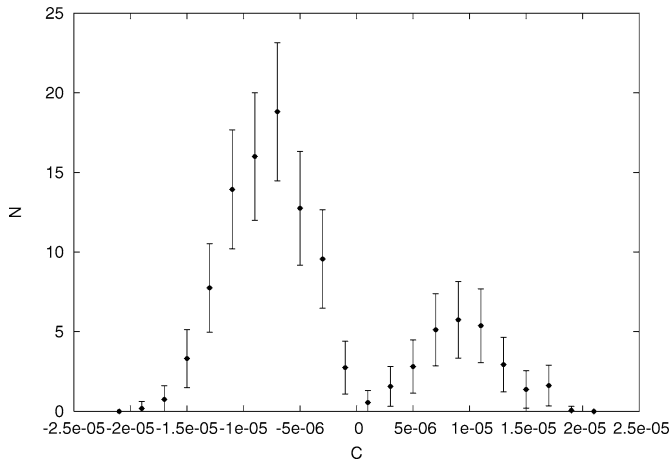


Fig. 17. Symbols show number $N_{\text{obs}}(C)$ of observed Astrid members in $(C, C + \Delta C)$ bins with error-bars given as $\sqrt{N_{\text{obs}}(C)}$. We chose $\Delta C = 2 \times 10^{-6}$ AU and a_c uniformly averaged in the range (2.785, 2.788) AU. In this case, $N(C)$ is not symmetric about $C = 0$, with number of asteroids for positive C systematically smaller. In Section 5.4 we consider possibilities for this asymmetry and in the further analysis we use the $C < 0$ part of the data only.

metric about $C = 0$ (with only $\sim 5\%$ less bodies for $C > 0$), as if the rate of asteroid elimination from the family by the 3J–1S–1 resonance was smaller than that found in our simulation. It is possible, however, that some asteroids were initially thrown beyond this resonance and thus avoided interacting with it altogether.

5.4. Astrid

The primary enigma of the Astrid family stems from its asymmetry in $N_{\text{obs}}(C)$ about $C = 0$, or in other words its asymmetry in a about $a_c \simeq 2.787$ AU (position of 1128 Astrid; Fig. 10). There are no meaningful mean motion resonances crossing this family to trigger depletion for $a \geq a_c$. We note that the powerful J5/2 mean motion resonance with Jupiter is nearby, but its separatrix at ~ 2.82 AU is more than ~ 0.015 AU from the closest Astrid members. Thus, the majority of this family is well separated from this resonance. Even more puzzling is that fact that the zone between the Astrid family and the J5/2 resonance is empty of any (family or background) objects.

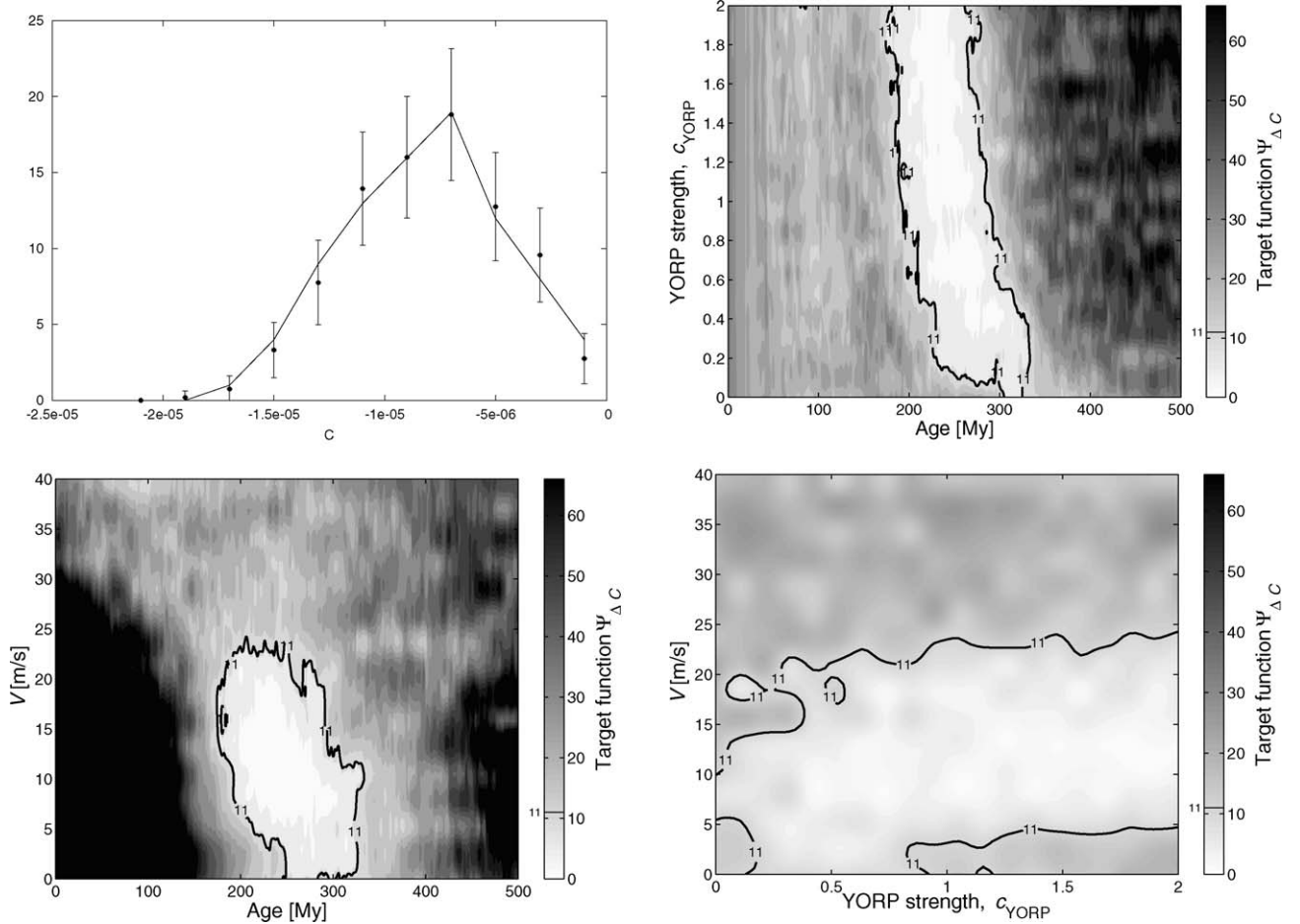


Fig. 18. Results of our simulation for the Astrid family with mean albedo $p_V = 0.08$ and surface thermal conductivity $K = 0.05$ W/m/K. Top and left is the best-fit simulation of number of asteroids $N(C)$ in the C -bins (solid line) compared to the observed family $N_{\text{obs}}(C)$ (symbols and error-bars). Top and right, and bottom figures show projection of the best value of the target function $\Psi_{\Delta C}$ for various pairs of the solved-for parameters: (i) age T vs YORP strength parameter c_{YORP} , (ii) age T vs characteristic velocity V of initial ejection of $D = 5$ km fragments, and (iii) c_{YORP} vs V . The critical-level contour $\Psi_{\Delta C} = a + 3 = 11$, a is the number of degrees of freedom, that serves to estimate uncertainties of the solved-for parameters is shown in bold; other values of the target function are shown in scales of gray.

At first, we suspected there might be a more complex resonance—such as the high-order secular resonance—near the Astrid family that could quickly transport objects into the $J5/2$ mean motion resonance and thus provide significant depletion. Our direct numerical simulation of 110 Astrid asteroids and their clones, however, does not support this idea. In Fig. 22, we show evolutionary tracks of these particles integrated over 200 Myr. Their sizes range from $D = 3$ to 12 km and their obliquities were set to $\sim 45^\circ$ to force them to migrate toward the $J5/2$ resonance. Except for the effects of a few very weak resonances, we do not detect any noticeable perturbation prior to them falling into the $J5/2$. From the dynamical standpoint, the Astrid family should thus be able to extend much further toward the $J5/2$ resonance than observations suggest (we also repeated this simulation with the direct dynamical effects of the inner planets but did not find any significant change).

Note that migration toward higher a values requires a prograde spin state. Using the same integrator as that described in Vokrouhlický et al. (2003), we checked that there is no instability in the prograde-rotation states of Astrid family members. In fact, the phase space of rotation states looks very similar to

that of Koronis family members, who are also located near the $J5/2$ resonance. In this region, prograde rotation states are frequently trapped in “Slivan states” within the spin-orbit secular resonance s_6 . We speculate that a similar situation might arise for Astrid family members, whose obliquities become trapped near $\sim 50^\circ$; this would prevent them from migrating at their maximum da/dt rate. This factor might also contribute to the asymmetry seen in the family.

On the other hand, migration toward higher a values is not prohibited in this scenario. At best, we would still expect the population with $a \leq a_c$ to only be a factor of 2 or so higher than those with $a \geq a_c$. We cannot rule out the possibility that initial velocity field and/or the initial spin axis distribution was highly anisotropic, but neither answer seems particularly satisfying. A detailed study of this issue is beyond the scope of this paper.

Note that results from Nesvorný and Bottke (2004) indicate that a statistical majority of Karin family asteroids migrated toward the Sun during the past 5.8 Myr. They proposed that this could signify unequal angular momentum distribution among the observed fragments produced by the disruption of Karin’s

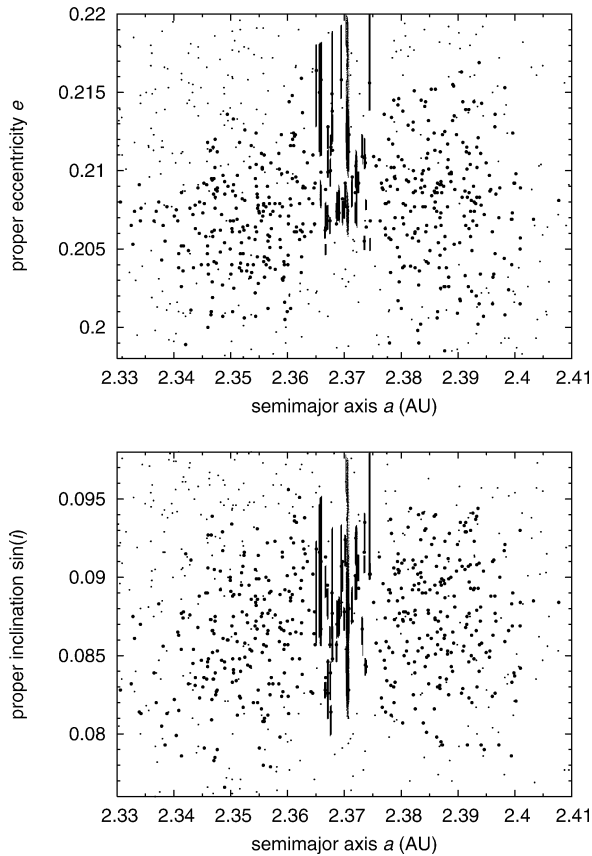


Fig. 19. Evolution tracks of a sample of numerically integrated orbits without Yarkovsky forces in the Erigone family: (i) proper semimajor axis a vs proper eccentricity e (top), and (ii) proper semimajor axis a vs proper sine of inclination $\sin i$ (bottom). Initial data of 108 selected real members, and their close clones, chosen near the center of the family, where depletion is observed. Integration timespan has been set to 500 Myr, more than the estimated age of the family from Fig. 13. The orbits are stable indicating no macroscopic chaos that could be associated with any of the weak mean motion resonances. The larger observed variations in proper eccentricity and inclination is due to interaction with the z_2 secular resonance. This effect is however very stable on a long-term. As a result, the observed depletion is unlikely to be explained by chaotic leakage from the central zone in the family, rather it follows from synergy of the Yarkovsky/YORP evolution discussed earlier in this paper.

parent body (see Paolicchi, 2005). Perhaps something similar happened to the Astrid family. Alternatively, Astrid members (and perhaps Karin family members) may be devoid of regolith and thus could have unusually high thermal conductivity values. This would allow them to evolve predominantly by the seasonal variant of the Yarkovsky effect, which only drives bodies toward the Sun (see already Farinella and Vokrouhlický, 1999). We find this idea more plausible, however, for the 5.8 Myr old Karin family than the older and presumably more heavily impacted Astrid family, which likely has formed some regolith since its formation.

6. Discussion

In this paper, we studied the structure of 4 young families and demonstrated that a combined Yarkovsky/YORP evolution model can be used to constrain their ages and other important properties. The ages are the best available to date, though

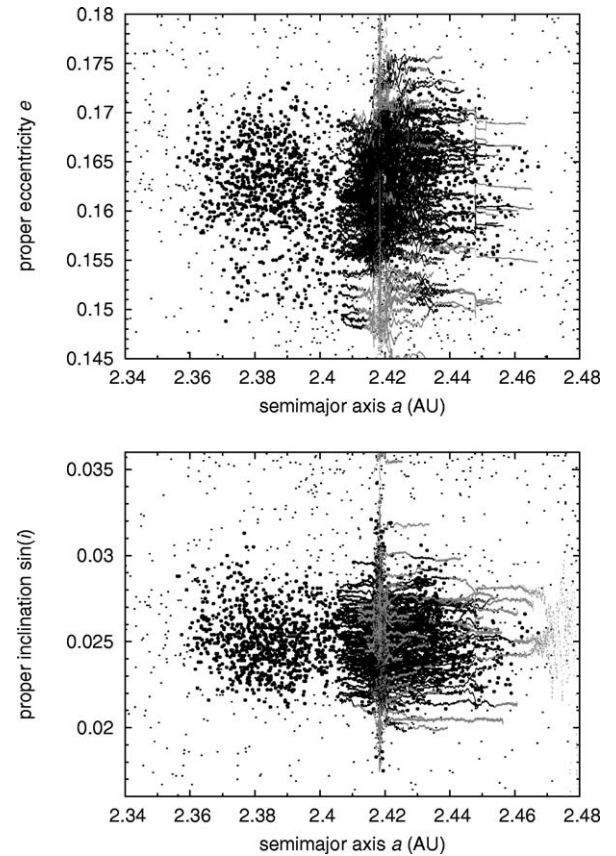


Fig. 20. Evolution tracks of a sample of numerically integrated orbits with Yarkovsky forces in the Massalia family: (i) proper semimajor axis a vs proper eccentricity e (top), and (ii) proper semimajor axis a vs proper sine of inclination $\sin i$ (bottom). Initial data of 137 selected real members chosen near the center of the family. Obliquities, roughly set to 45° , make the bodies migrate toward larger values of the semimajor axis, and the integration spans 240 Myr. Upon reaching the position of the exterior M1/2 mean motion resonance with Mars, the proper e and proper $\sin i$ are partly dispersed. The black tracks are for bodies that would be still associated with the observed Massalia family at the nominal HCM velocity cut-off $V_c = 44$ m/s; the gray sections correspond to a configuration, when the body ceases to be HCM-associated with the nominal family. Some 16% of bodies leaked from the family via this process in our simulation.

there are uncertainties based in part on the unknown surface parameters of the member asteroids (i.e., albedo and thermal conductivity) and also due to unavoidable uncertainties in the proper identification of the family.

We find it interesting that our search has found two families—Erigone and Merxia—with parent bodies marginally larger than 100 km and ages <0.5 Gyr. Moreover, the Veritas family is a borderline case between a cratering and catastrophic disruption event with an age of 8.3 Myr (Nesvorný et al., 2003). The Massalia case, while interesting, can be considered a large cratering event. We believe our search for such events is nearly complete, though it is possible that we missed one or two cases because mean motion resonances cut the relevant families into pieces and prevented the application of our method. This number compares rather well with recent work by Bottke et al. (2005a, 2005b), who found using collisional models of the main belt that ~ 4 asteroid families with parent bodies larger than 100 km should have been created over the past 1 Gyr.

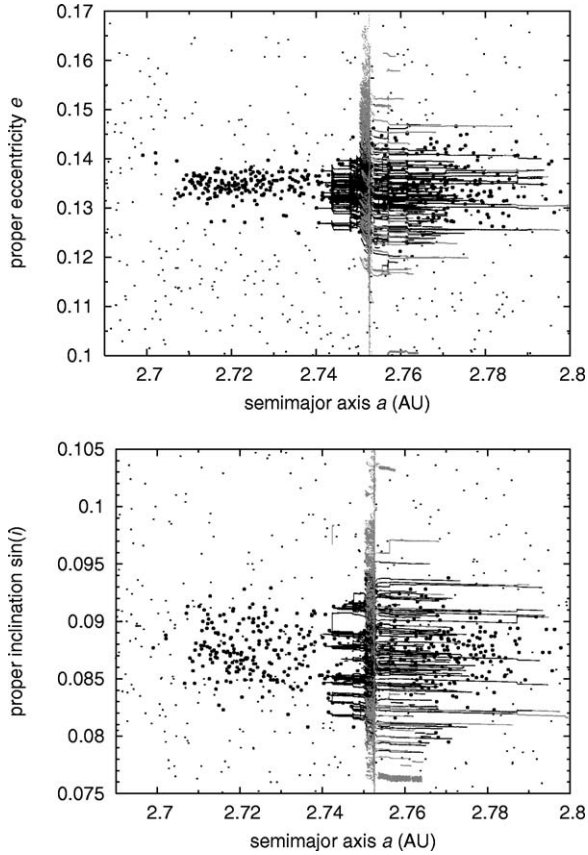


Fig. 21. Evolution tracks of a sample of numerically integrated orbits with Yarkovsky forces in the Merxia family: (i) proper semimajor axis a vs proper eccentricity e (top), and (ii) proper semimajor axis a vs proper sine of inclination $\sin I$ (bottom). Initial data of 145 selected real members, and their close clones, chosen near the center of the family. Obliquities, roughly set to 45° , make the bodies migrate toward larger values of the semimajor axis, and the integration spans 250 Myr. Upon reaching the position of the three-body 3J–1S–1 resonance the proper e and proper $\sin I$ are partly dispersed. The black tracks are for bodies that would be still associated with the observed Massalia family at the nominal HCM velocity cut-off $V_c = 80$ m/s; the gray sections correspond to a configuration, when the body ceases to be HCM-associated with the nominal family. After crossing the resonance, the proper e and proper $\sin I$ dispersion in the family increases to a level compatible with the observed members.

An compelling starting point for the future research may be to understand whether the paucity of > 100 km parent-body families with ages in between 0.5 and 1 Gyr is a statistical fluke, or whether it points instead to some missing element in our model.

It is interesting to note how the derived initial velocity fields for our families and their related initial dispersion in a compare with their observed dispersion in eccentricity e and inclination I . In the case of young families, where resonant diffusive effects are limited, we would ideally like to use the derived characteristic velocity V values to recover the observed e and I dispersions. To perform this comparison, we must first determine a characteristic size for observed family members in each of our 4 families. Using the estimated mean albedo values above, we obtained the following values: Erigone $D \simeq 2$ –2.5 km, Massalia $D \simeq 1$ –1.5 km, Merxia $D \simeq 1.5$ –2 km, and Astrid $D \simeq 3$ km. With those values, and the assumed $V_{SD} \propto 1/D$ velocity scaling (note our determined

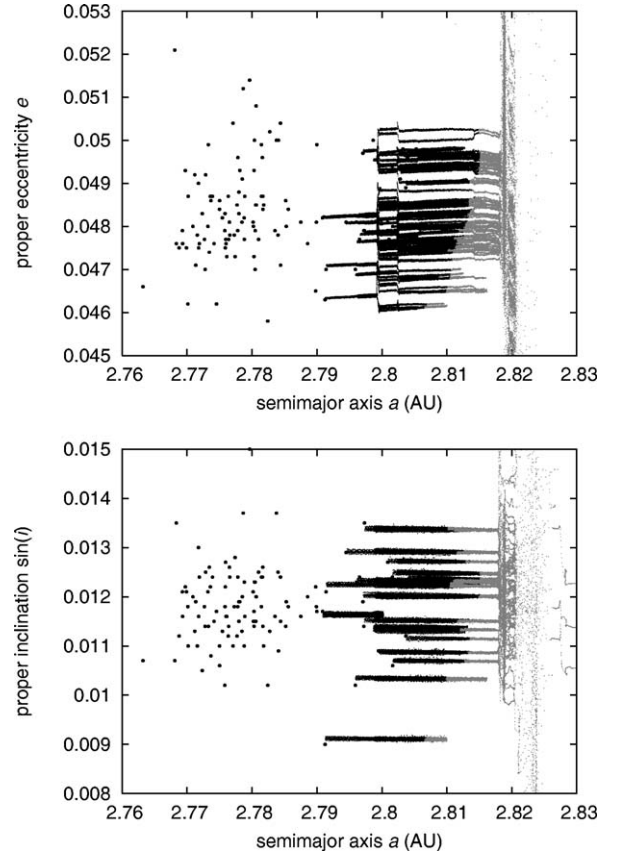


Fig. 22. Evolution tracks of a sample of numerically integrated orbits with Yarkovsky forces in the Astrid family: (i) proper semimajor axis a vs proper eccentricity e (top), and (ii) proper semimajor axis a vs proper sine of inclination $\sin I$ (bottom). Initial data of 110 selected real members, and their close clones, chosen near the center of the family. Obliquities, roughly set to 45° , make the bodies migrate toward larger values of the semimajor axis. The orbits continue quietly migrating until they reach separatrix of the J5/2 mean motion resonance with Jupiter where they are eliminated. At this level of sophistication, there is no sign why the zone between the observed Astrid family and the separatrix of the J5/2 should be prohibited; yet no asteroids—family or background—are observed in this zone.

velocities V are for $D = 5$ km size fragments), we computed their maximum e and I dispersions from the Gauss equations (e.g., Zappalà et al., 1996): $\Delta e \simeq 0.016$ and $\Delta \sin I \simeq 0.008$ for Erigone and Merxia, $\Delta e \simeq 0.014$ and $\Delta \sin I \simeq 0.008$ for Massalia, $\Delta e \simeq 0.005$ and $\Delta \sin I \simeq 0.003$ for Astrid. The actual dispersion should be somewhat smaller because it depends on the parent body's a priori unknown angular parameters ω , the argument of pericenter, and f , the true anomaly (Zappalà et al., 1996). Comparing these values with our family data, we find modest agreement. Our expected inclination dispersion is short in a few cases by a factor of 1.5–2. Our expected eccentricity dispersion is comparable to observation for Erigone and Merxia, while it falls short by a factor of about 1.5 for Massalia and Astrid.

It is plausible that the mismatches were produced by initial velocity fields that were anisotropic, with larger dispersions occurring along the e and I directions. This conclusion was reached using the following observations. First, an analysis of the collisional geometry between asteroids in the main belt in-

dicates that the along-track relative velocity of the target and projectile is statistically smaller than both the radial and normal components of the relative velocity. In particular, the normal component (responsible for the inclination dispersion) is found up to a factor 2–5 larger than the along-track component (depending on location of the target body; e.g., Bottke et al., 1994). Second, numerical simulations of catastrophic disruptions of large asteroids indicate that anisotropy in the ejecta velocity field is usually produced along the axis of the projectile’s impact velocity vector (e.g., Durda et al., 2004). Thus, for non-zero inclination impacts, an irregular spray of ejecta may sample different directions with a slight preference for the projectile’s trajectory. A combination of these two effects may explain the initial dispersion of the asteroid families in e and I as compared to the reconstructed initial dispersion in a .

Can our method be applied to older families? At present, our method requires that we meet certain conditions that are not satisfied in all of the known families. Our method has been used to estimate the age of the Eos family, whose orbital distribution is similar to those families described in this paper (Vokrouhlický et al., 2005). Other families with comparable shapes (e.g., Agnia, Naema), however, require additional care. The Agnia family is fully embedded inside the high-order secular resonance z_1 (e.g., Milani and Knežević, 1994; Vokrouhlický et al., in preparation), which may strongly affect its dynamical evolution. It is also a small family, with a parent body only a few tens of kilometers in size. This means that many of its members, like the members of the Astrid family, are small and hard to detect. Further discoveries and proper element computations will help to define these families better than we can today.

Second, there are two age regimes where our method has not yet been adapted, at least in the present formulation. Very young families with ages less than $\simeq 50$ Myr (e.g., Karin, Veritas, or Iannini) have not evolved enough by Yarkovsky/YORP thermal forces to produce the required offset in the extremes of their $N_{\text{obs}}(C)$ distributions; these offsets are needed to compute an age. Obviously, the thermal forces do perturb all asteroid orbits, including those in the very young families, but the means to detect them are different than that used here (see Nesvorný and Bottke, 2004). Conversely, older families with ages > 1 Gyr appear to have evolved so much by thermal forces that the assumptions implicit in our model begin to breakdown.

A good example of the latter occurs in the Themis family, whose age is estimated to be $\sim(2.5 \pm 1.0)$ Gyr (e.g., Nesvorný et al., 2005) and whose projection onto the proper semimajor axis a vs absolute magnitude H is shown in Fig. 23. The family is bracketed by powerful mean motion resonances (J2/1, J11/5, and 3J–2S–1). One can also see the distinct feature of a relative under-population in the middle- a values and a relative overpopulation in the extreme- a values for asteroids with $H \geq 12.5$. To understand why our model has problems with this family, recall that these features result from a synergy between Yarkovsky-driven secular changes in a enhanced by the YORP-driven tilting of the spin axes toward extreme obliquity values. As those asymptotic values are reached, the YORP effect continues to either accelerate or decelerate an asteroid’s rotation rate to the point where the rotation state undergoes a dramatic

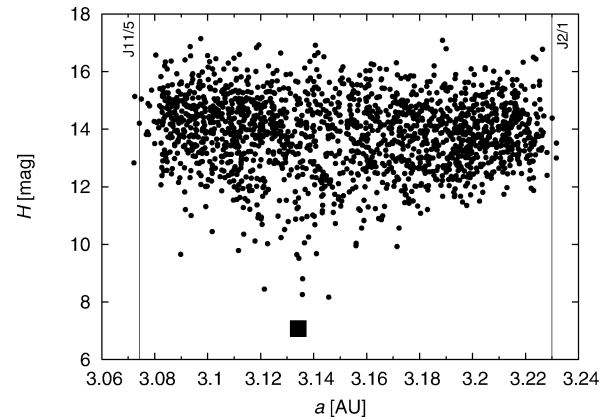


Fig. 23. Themis family identified with the HCM cut-off velocity $V_c = 58$ m/s projected onto a plane of proper semimajor axis a and absolute magnitude H . Filled square is (24) Themis.

change either by collisional impact, structural alterations, or fission. At this time, we do not understand these “end-states” well enough to model them correctly.

Vokrouhlický and Čapek (2002) and Čapek and Vokrouhlický (2004) estimated that the typical timescale for a so-called “YORP cycle” among ~ 5 km objects is ~ 300 – 600 Myr. For the families studied in Section 4, their age is about the length of the YORP cycle for those asteroids defining the $N_{\text{obs}}(C)$ distribution. As such, our age estimates are not seriously affected by our inability to accurately model the termination of the YORP cycle as well as the onset of a new YORP cycle. For a ~ 2.5 Gyr old family such as Themis, however, one could expect small members to have experienced 5 to 8 YORP cycles during the family’s lifetime. Accordingly, our inability to accurately model multiple YORP cycles could lead to inaccurate age determination results. For instance, if we formally attempt to use our present method in the Themis family case, we would obtain a poor fit (i.e., the minimum value of the target function $\Psi_{\Delta C}$ would be larger than number of data points).

One possible way to improve our model for older families might be to relax those parameters affecting the collisional re-orientation timescale τ_{reor} from Eq. (11). This issue is closely related to the problem of YORP cycle termination because asteroids spun down by YORP may presumably be spun up once again by non-disruptive collisional impacts. Note that the true value of τ_{reor} is poorly understood; current estimates rely on analytical approximations rather than more realistic hydrocode simulations of asteroid impacts. This remains an important area for new work.

Finally, our work confirms that the families studied in this paper have small initial dispersal velocities. A typical velocity V for ~ 5 km fragments was found to be a few tens of meters per second. This value is compatible with hydrocode simulation of asteroid impacts. It also means that the initial semimajor axis dispersion for the families described here was ~ 30 – 50% of the observed value.

Acknowledgments

This work has been supported by the Grant Agency of the Czech Republic (D.V. and M.B.; Grant 205/05/2737) and

NASA's Planetary Geology & Geophysics program (W.F.B. and D.N.). We thank M. Čuk, P. Paolicchi and F. Roig whose comments helped to improve the original version of this paper.

References

- Asphaug, E., 1997. Impact origin of the Vesta family. *Meteor. Planet. Sci.* 32, 965–980.
- Bahcall, J.N., Pinsonneault, M.H., Basu, S., 2001. Solar models: Current epoch and time dependences, neutrinos, and helioseismological properties. *Astrophys. J.* 555, 990–1012.
- Belton, M.J.S., Veverka, J., Thomas, P., Helfenstein, P., Simonelli, D., Chapman, C., Davies, M.E., Greeley, R., Greenberg, R., Head, J., 1992. Galileo encounter with 951 Gaspra—First pictures of an asteroid. *Science* 257, 1647–1652.
- Belton, M.J.S., and 19 colleagues, 1994. First images of Asteroid 243 Ida. *Science* 265, 1543–1547.
- Bendjoya, P., Zappalà, V., 2002. Asteroid family identification. In: Bottke, W.F., Cellino, A., Paolicchi, P., Binzel, R.P. (Eds.), *Asteroids III*. Univ. of Arizona Press, Tucson, pp. 613–618.
- Benz, W., Asphaug, E., 1999. Catastrophic disruptions revisited. *Icarus* 142, 5–20.
- Bertotti, B., Farinella, P., Vokrouhlický, D., 2003. *Physics of the Solar System*. Kluwer Academic, Dordrecht.
- Bottke, W.F., Nolan, M.C., Greenberg, R., Kolvoord, R.A., 1994. Velocity distributions among colliding asteroids. *Icarus* 107, 255–268.
- Bottke, W.F., Vokrouhlický, D., Brož, M., Nesvorný, D., Morbidelli, A., 2001. Dynamical spreading of asteroid families via the Yarkovsky effect: The Koronis family and beyond. *Science* 294, 1693–1695.
- Bottke, W.F., Vokrouhlický, D., Rubincam, D.P., Brož, M., 2002. Dynamical evolution of asteroids and meteoroids using the Yarkovsky effect. In: Bottke, W.F., Cellino, A., Paolicchi, P., Binzel, R.P. (Eds.), *Asteroids III*. Univ. of Arizona Press, Tucson, pp. 395–408.
- Bottke, W.F., Durda, D.D., Nesvorný, D., Jedicke, R., Morbidelli, A., Vokrouhlický, D., Levison, H.F., 2005a. The fossilized size distribution of the main asteroid belt. *Icarus* 175, 111–140.
- Bottke, W.F., Durda, D.D., Nesvorný, D., Jedicke, R., Morbidelli, A., Vokrouhlický, D., Levison, H.F., 2005b. Linking the collisional history of the main asteroid belt to its dynamical excitation and depletion. *Icarus* 179, 63–94.
- Brouwer, D., 1951. Secular variations of the orbital elements of minor planets. *Astron. J.* 56, 9–32.
- Bus, S.J., Binzel, R.P., 2002. Phase II of the small main-belt asteroid spectroscopic survey. The observations. *Icarus* 158, 106–145.
- Čapek, D., Vokrouhlický, D., 2004. The YORP effect with finite thermal conductivity. *Icarus* 172, 526–536.
- Carruba, V., Burns, J.A., Bottke, W.F., Nesvorný, D., 2003. Orbital evolution of the Gefion and Adeona asteroid families: Close encounters with massive asteroids and the Yarkovsky effect. *Icarus* 162, 308–327.
- Carruba, V., Michtchenko, T.A., Roig, F., Ferraz-Mello, S., Nesvorný, D., 2005. On the V-type asteroids outside the Vesta family. I. Interplay of nonlinear secular resonances and the Yarkovsky effect: The cases of 956 Elisa and 809 Lundia. *Astron. Astrophys.* 441, 819–830.
- Cellino, A., Michel, P., Tanga, P., Zappalà, V., Paolicchi, P., Dell'Oro, A., 1999. The velocity–size relationship for members of asteroid families and implications for the physics of catastrophic collisions. *Icarus* 141, 79–95.
- Cellino, A., Bus, S.J., Doressoundiram, A., Lazzaro, D., 2002. Spectroscopic properties of asteroid families. In: Bottke, W.F., Cellino, A., Paolicchi, P., Binzel, R.P. (Eds.), *Asteroids III*. Univ. of Arizona Press, Tucson, pp. 633–643.
- Chapman, C.R., 2002. Cratering on asteroids from Galileo and NEAR Shoemaker. In: Bottke, W.F., Cellino, A., Paolicchi, P., Binzel, R.P. (Eds.), *Asteroids III*. Univ. of Arizona Press, Tucson, pp. 315–330.
- Chapman, C.R., 2004. Space weathering of asteroid surfaces. *Annu. Rev. Earth Planet. Sci.* 32, 539–567.
- Chapman, C.R., Ryan, E.V., Merline, W.J., Neukum, G., Wagner, R., Thomas, P.C., Veverka, J., Sullivan, R.J., 1996a. Cratering on Ida. *Icarus* 120, 77–86.
- Chapman, C.R., Veverka, J., Belton, M.J.S., Neukum, G., Morrison, D., 1996b. Cratering on Gaspra. *Icarus* 120, 231–245.
- Dell'Oro, A., Bigongiari, G., Paolicchi, P., Cellino, A., 2004. Asteroid families: Evidence of aging of the proper elements. *Icarus* 169, 341–356.
- Dohnányi, J.W., 1969. Collisional models of asteroids and their debris. *J. Geophys. Res.* 74, 2531–2554.
- Durda, D.D., Bottke, W.F., Enke, B.L., Merline, W.J., Asphaug, E., Richardson, D.C., Leinhardt, Z.M., 2004. The formation of asteroid satellites in large impacts: Results from numerical simulations. *Icarus* 167, 382–396.
- Farinella, P., Vokrouhlický, D., 1999. Semimajor axis mobility of asteroidal fragments. *Science* 283, 1507–1510.
- Farinella, P., Carpino, M., Froeschlé, Ch., Froeschlé, C., Gonczi, R., Knežević, Z., Zappalà, V., 1989. The ages of asteroid families. *Astron. Astrophys.* 217, 298–306.
- Farinella, P., Vokrouhlický, D., Hartmann, W.K., 1998. Meteorite delivery via Yarkovsky orbital drift. *Icarus* 132, 378–387.
- Greenberg, R., Nolan, M.C., Bottke, W.F., Kolvoord, R.A., Veverka, J., 1994. Collisional history of Gaspra. *Icarus* 107, 84–97.
- Greenberg, R., Bottke, W.F., Nolan, M.C., Geissler, P., Petit, J., Durda, D.D., Asphaug, E., Head, J., 1996. Collisional and dynamical history of Ida. *Icarus* 120, 106–118.
- Ivezić, Z., and 32 colleagues, 2001. Solar System objects observed in the Sloan Digital Sky Survey commissioning data. *Astron. J.* 122, 2749–2784.
- Jedicke, R., Nesvorný, D., Whiteley, R., Ivezić, Z., Jurić, M., 2004. An age–color relationship for main-belt S-complex asteroids. *Nature* 429, 275–277.
- Jurić, M., and 12 colleagues, 2002. Comparison of positions and magnitudes of asteroids observed in the Sloan Digital Sky Survey with those predicted for known asteroids. *Astron. J.* 124, 1776–1787.
- Knežević, Z., Milani, A., 2000. Synthetic proper elements for outer main-belt asteroids. *Celest. Mech. Dynam. Astron.* 78, 17–46.
- Knežević, Z., Milani, A., 2003. Proper element catalogs and asteroid families. *Astron. Astrophys.* 403, 1165–1173.
- Knežević, Z., Lemaître, A., Milani, A., 2002. The determination of asteroid proper elements. In: Bottke, W.F., Cellino, A., Paolicchi, P., Binzel, R.P. (Eds.), *Asteroids III*. Univ. of Arizona Press, Tucson, pp. 603–612.
- Laskar, J., Robutel, P., 2001. High order symplectic integrators for perturbed Hamiltonian systems. *Celest. Mech. Dynam. Astron.* 80, 39–62.
- Levison, H., Duncan, M., 1994. The long-term dynamical behavior of short-period comets. *Icarus* 108, 18–36.
- Love, S.G., Ahrens, T.J., 1996. Catastrophic impacts on gravity dominated asteroids. *Icarus* 124, 141–155.
- Marzari, F., Davis, D.R., Vanzani, V., 1995. Collisional evolution of asteroid families. *Icarus* 113, 168–187.
- Marzari, F., Cellino, A., Davis, D.R., Farinella, P., Zappalà, V., Vanzani, V., 1996. Origin and evolution of the Vesta asteroid family. *Astron. Astrophys.* 316, 248–262.
- Marzari, F., Farinella, P., Davis, D.R., 1999. Origin, aging, and death of asteroid families. *Icarus* 142, 63–77.
- Michel, P., Benz, W., Tanga, P., Richardson, D.C., 2001. Collisions and gravitational reaccumulation: Forming asteroid families and satellites. *Science* 294, 1696–1700.
- Michel, P., Tanga, P., Benz, W., Richardson, D.C., 2002. Formation of asteroid families by catastrophic disruption: Simulations with fragmentation and gravitational reaccumulation. *Icarus* 160, 10–23.
- Migliorini, F., Zappalà, V., Vio, R., Cellino, A., 1995. Interlopers within asteroid families. *Icarus* 118, 271–291.
- Milani, A., Farinella, P., 1994. The age of Veritas asteroid family deduced by chaotic chronology. *Nature* 370, 40–42.
- Milani, A., Knežević, Z., 1992. Asteroid proper elements and secular resonances. *Icarus* 98, 211–232.
- Milani, A., Knežević, Z., 1994. Asteroid proper elements and the dynamical structure of the asteroid main belt. *Icarus* 107, 219–254.
- Morbidelli, A., Nesvorný, D., 1999. Numerous weak resonances drive asteroids toward terrestrial planets orbits. *Icarus* 139, 295–308.
- Morbidelli, A., Nesvorný, D., Bottke, W.F., Michel, P., Vokrouhlický, D., Tanga, P., 2003. The shallow magnitude distribution of asteroid families. *Icarus* 162, 328–336.
- Mothé-Diniz, T., Roig, F., Carvano, J.M., 2005. Reanalysis of asteroid families structure through visible spectroscopy. *Icarus* 174, 54–80.
- Nesvorný, D., Bottke, W.F., 2004. Detection of the Yarkovsky effect for main-belt asteroids. *Icarus* 170, 324–342.

- Nesvorný, D., Morbidelli, A., 1998. Three-body mean motion resonances and the chaotic structure of the asteroid belt. *Astron. J.* 116, 3029–3037.
- Nesvorný, D., Morbidelli, A., Vokrouhlický, D., Bottke, W.F., Brož, M., 2002a. The Flora family: A case of the dynamically dispersed collisional swarm? *Icarus* 157, 155–172.
- Nesvorný, D., Bottke, W.F., Dones, L., Levison, H.F., 2002b. The recent breakup of an asteroid in the main-belt region. *Nature* 417, 720–722.
- Nesvorný, D., Bottke, W.F., Levison, H.F., Dones, L., 2003. Recent origin of the Solar System dust bands. *Astrophys. J.* 591, 486–497.
- Nesvorný, D., Jedicke, R., Whiteley, R.J., Ivezić, Ž., 2005. Evidence for asteroid space weathering from the Sloan Digital Sky Survey. *Icarus* 173, 132–152.
- Paolicchi, P., 2005. Rotational properties of asteroids: A tool to understand their evolution? *Mem. Soc. Astron. Italiana Suppl.* 6, 110–115.
- Petit, J.-M., Farinella, P., 1993. Modeling the outcomes of high-velocity impacts between small Solar System bodies. *Celest. Mech. Dynam. Astron.* 57, 1–28.
- Press, W.H., Teukolsky, S.A., Vetterlink, W.T., Flannery, B.P., 1999. *Numerical Recipes in Fortran 77*. Cambridge Univ. Press, Cambridge.
- Roig, F., Gil-Hutton, R., 2006. Selecting candidate V type asteroids from the analysis of the Sloan Digital Sky Survey colors. *Icarus*. Submitted for publication.
- Rubincam, D.P., 2000. Radiative spin-up and spin-down of small asteroids. *Icarus* 148, 2–11.
- Ryan, E.V., Melosh, H.J., 1998. Impact fragmentation: From the laboratory to asteroids. *Icarus* 133, 1–24.
- Šidlichovský, M., Nesvorný, D., 1997. Frequency modified Fourier transform and its applications to asteroids. *Celest. Mech. Dynam. Astron.* 65, 137–148.
- Slivan, S.M., 2002. Spin vector alignment of Koronis family asteroids. *Nature* 419, 49–51.
- Slivan, S.M., Binzel, R.P., Crespo da Silva, L.D., Kaasalainen, M., Lyndaker, M.M., Krčo, M., 2003. Spin vectors in the Koronis family: Comprehensive results from two independent analyses of 213 rotation lightcurves. *Icarus* 162, 285–307.
- Tanga, P., Cellino, A., Michel, P., Zappalà, V., Paolicchi, P., Dell’Oro, A., 1999. On the size distribution of asteroid families: The role of geometry. *Icarus* 141, 65–78.
- Tedesco, E.F., Noah, P.V., Noah, M., Price, S.D., 2002. The supplemental IRAS minor planet survey. *Astron. J.* 123, 1056–1085.
- Veverka, J., and 11 colleagues, 1994. Discovery of grooves on Gaspra. *Icarus* 107, 72–83.
- Vokrouhlický, D., 1998. Diurnal Yarkovsky effect as a source of mobility of meter-sized asteroidal fragments. I. Linear theory. *Astron. Astrophys.* 335, 1093–1100.
- Vokrouhlický, D., 1999. A complete linear model for the Yarkovsky thermal force on spherical asteroid fragments. *Astron. Astrophys.* 344, 362–366.
- Vokrouhlický, D., Brož, M., 2002. Interaction of the Yarkovsky-drifting orbits with weak resonances: Numerical evidence and challenges. In: Cellletti, A., Ferraz-Mello, S., Henrard, J. (Eds.), *Modern Celestial Mechanics: From Theory to Applications*. Kluwer Academic, Dordrecht, pp. 467–472.
- Vokrouhlický, D., Čapek, D., 2002. YORP-induced long-term evolution of the spin state of small asteroids and meteoroids. Rubincam’s approximation. *Icarus* 159, 449–467.
- Vokrouhlický, D., Farinella, P., 1998. The Yarkovsky seasonal effect on asteroidal fragments: A nonlinearized theory for the plane-parallel case. *Astron. J.* 116, 2032–2041.
- Vokrouhlický, D., Farinella, P., 1999. The Yarkovsky seasonal effect on asteroidal fragments: A nonlinearized theory for spherical bodies. *Astron. J.* 118, 3049–3060.
- Vokrouhlický, D., Brož, M., Morbidelli, A., Bottke, W.F., Nesvorný, D., Lazaro, D., Rivkin, A.S., 2002. Yarkovsky footprints in the Eos family. Presented at the Asteroids, Comets and Meteors Meeting, Berlin. Abstract 12.01.
- Vokrouhlický, D., Nesvorný, D., Bottke, W.F., 2003. Thermal torques produce spin vector alignments among Koronis family asteroids. *Nature* 425, 147–151.
- Vokrouhlický, D., Brož, M., Morbidelli, A., Bottke, W.F., Nesvorný, D., Lazaro, D., Rivkin, A.S., 2005. Yarkovsky footprints in the Eos family. *Icarus*. In press.
- Zappalà, V., Cellino, A., Farinella, P., Knežević, Z., 1990. Asteroid families. I. Identification by hierarchical clustering and reliability assessment. *Astron. J.* 100, 2030–2046.
- Zappalà, V., Bendjoya, P., Cellino, A., Farinella, P., Froeschlé, C., 1995. Asteroid families: Search of a 12,487-asteroid sample using two different clustering techniques. *Icarus* 116, 291–314.
- Zappalà, V., Cellino, A., Dell’Oro, A., Migliorini, F., Paolicchi, P., 1996. Reconstructing the original velocity fields of asteroid families. *Icarus* 124, 156–180.
- Zappalà, V., Cellino, A., Dell’Oro, A., Paolicchi, P., 2002. Physical and dynamical properties of asteroid families. In: Bottke, W.F., Cellino, A., Paolicchi, P., Binzel, R.P. (Eds.), *Asteroids III*. Univ. of Arizona Press, Tucson, pp. 619–631.